Title

GJA1 Depletion Causes Ciliary Defects by Affecting Rab11 Trafficking to the Ciliary Base.

Author names and affiliations

Dong Gil Jang[1], Keun Yeong Kwon[1], Yeong Cheon Kweon[1], Byung-gyu Kim[2], Kyungjae Myung[2], Hyun-Shik Lee[3], Chan Young Park[1], Taejoon Kwon[2,4,*] and Tae Joo Park[1,2,*]

[1] Department of Biological Sciences, College of Information-Bio Convergence Engineering, Ulsan National Institute of Science and Technology, Ulsan 44919, Republic of Korea.

[2] Center for Genomic Integrity, Institute for Basic Science, Ulsan 44919, Republic of Korea

[3] KNU-Center for Nonlinear Dynamics, CMRI, School of Life Sciences, BK21 Plus KNU Creative Bio Research Group, College of Natural Sciences, Kyungpook National University, Daegu 41566, Republic of Korea

[4] Department of Biomedical Engineering, College of Information-Bio Convergence Engineering, Ulsan National Institute of Science and Technology, Ulsan 44919, Republic of Korea.

[*] Corresponding author

Abstract

The gap junction complex functions as a transport channel across the membrane. Among gap junction subunits, gap junction protein alpha 1 (GJA1) is the most commonly expressed subunit. However, the roles of GJA1 in the formation and function of cilia remain unknown. Here, we examined GJA1 functions during ciliogenesis in vertebrates. GJA1 was localized to the motile ciliary axonemes or pericentriolar material (PCM) around the primary cilium. GJA1 depletion caused the severe malformation of both primary cilium and motile cilia. Interestingly, GJA1 depletion caused strong delocalization of BBS4 from the PCM and basal body and distinct distribution as cytosolic puncta. Further, CP110 removal from the mother centriole was significantly reduced by GJA1 depletion. Importantly, Rab11, key regulator during ciliogenesis, was immunoprecipitated with GJA1 and GJA1 knockdown caused the mis-localization and mis-accumulation of Rab11. These findings suggest that GJA1 is necessary for proper ciliogenesis by regulating the Rab11 pathway.

Introduction

A gap junction, which is also known as a connexon, is a transmembrane (TM) protein complex that has an important role as a channel and transports low molecular compounds, nutrients, and ions across the lateral plasma membrane [1, 2]. It also regulates cell proliferation, differentiation, growth, and death [3-5]. A gap junction is composed of gap junction protein subunits, and there are five subgroups of gap junction protein families according to their homology in the amino acid sequence [6]. Twelve gap junction proteins make a gap junction complex, which consists of a combination taken from 21 different human gap junction proteins [7].

GJA1 (gap junction protein alpha 1), also known as CX43 (connexin 43kDa), was originally identified in a rat heart [8]. The human homologue of GJA1 is located at human chromosome 6q22-q23. The GJA1 gene was identified after discovering the putative genes for oculodentodigital dysplasia (ODDD) in human disease [9, 10]. Among all gap junction protein families, GJA1 is the

most common and a major subunit. It is expressed in many tissues, such as the eyes, ears, brain, and especially the heart [11-14].

The GJA1 protein has four TM domains with five linked subdomain loops. Among these loops, two loops are extracellular subdomains, and three loops, including the N- and C-terminal domain, are in the cytoplasm (Fig 1A) [15]. In the cytoplasm, the C-terminal domain of GJA1 regulates the cytoskeletal network (actin and tubulin [16]), cell extension, migration, and polarity [17-19]. A recent study reported that GJA1 also regulates the maintenance of cilia [20], which are microtubule-based cellular organelles that play crucial roles in the physiological maintenance of the human body [21]. However, the mechanisms and roles of GJA1 in the formation and function of cilia are yet to be determined.

Cilia exist in most types of vertebrate cells and are involved in various developmental processes and physiological responses from embryos to adults. For example, cilia are involved in cell cycle control, cell-to-cell signal transduction, fertilization, early embryonic development, extracellular environment sensing, and homeostasis [22]. Mutations in essential genes for cilia formation cause the disruption of ciliary structures or their functions and lead to “Ciliopathy”, which is an innate genetic and syndromic disorder [23, 24].

In this report, we discovered that GJA1 regulated ciliogenesis and was critical for early development. GJA1 localized not only at the gap junction, but also at the pericentriolar material (PCM) around the primary cilium of RPE1 cells and the ciliary axonemes in *Xenopus* epithelial tissues. The dominant-negative mutant-mediated dysfunction and antisense morpholino oligo (MO)-mediated knockdown of GJA1 caused severe malformation of motile cilia elongation and assembly in *Xenopus laevis*. Consistent with *Xenopus* model, siRNA-mediated-knockdown of GJA1 caused a reduction in primary cilia formation in human RPE1 cells.

Interestingly, GJA1 depletion caused strong delocalization of BBS4 from the PCM and basal bodies, and caused distinct distribution as cytosolic puncta. Further, CP110 removal from the mother centriole was significantly reduced by GJA1 depletion.

By performing immunoprecipitation (IP)-mass spectrometry (MS) analysis, we identified Rab11 and Rab8a as putative GJA1-binding partners. Rab11 was previously shown to be accumulated around the basal body, and is involved in the early steps of ciliogenesis [25, 26]. Further analysis showed that Rab11 was immunoprecipitated with GJA1, and knockdown of GJA1 in RPE1 cells resulted in the mis-localization of Rab11. These data suggest that GJA1 contributes to proper ciliogenesis by regulating Rab11 trafficking to basal bodies and facilitating ciliary axoneme formation and assembly.

Result

1. GJA1 localizes to the ciliary axonemes and basal bodies.

GJA1, which is a major component of the gap junction complex, consisted of four TM domains, interdomain loops between each TM, and intracellular N- and C- terminus domains (Fig 1A). To investigate the biological functions of GJA1 in the ciliogenesis of vertebrates, we cloned the *Xenopus laevis* homologue of human GJA1 based on the sequence from Xenbase [27]. Next, we analyzed GJA1 localization in multi-ciliated cells in *Xenopus* embryos by immunostaining for Flag-tagged GJA1 protein expression. Surprisingly, GJA1 localized to the ciliary components, such as basal bodies (Fig 1B', C', yellow arrow) and ciliary axonemes (Fig 1B', C', white arrow), in addition to the gap junction (Fig 1B, B' arrowhead) in *Xenopus* epithelial multi-ciliated cells. These data suggest that GJA1 may have roles in the ciliogenesis process.

2. Dominant-negative mutant-mediated dysfunction of GJA1 causes severe ciliary malformation in *Xenopus* epithelial tissue.

To determine the function of GJA1 during cilia formation, we exploited the dominant-negative mutants of GJA1. Two known dominant-negative mutants have been identified and frequently used in recent studies. The T154A point mutation mimics the closed-channel status of the gap junction complex but does not inhibit the formation of the gap junction [28]. The Δ130-136 deletion mutation

is a 7-amino acid deletion in the intracellular loop between TM 2 and 3. This mutation blocks gap junction permeability [29]. Lastly, we designed the Δ234-243 mutant, which is a 10-amino acid deletion in the putative tubulin-binding sequence of the C-terminus. This sequence only exists in GJA1 and is not conserved in other gap junction protein families (Fig 2A) [30]. Microinjection of each dominant-negative mutant at ventral-animal regions of two-cell stage embryos caused severe defects in cilia formation. Immunofluorescence analysis using an acetylated tubulin antibody showed severely shortened and less numbers of ciliary axonemes in dominant-negative mutant-injected embryos, compared to those of control embryos (Fig 2B). However, the basal bodies, which are the organizing center of ciliary axonemes, did not have noticeable defects, and the numbers of basal bodies and apical localization were comparable to those of controls (Fig 2B, green). Therefore, we focused on studying GJA1 functions for the ciliary axoneme formation phenotype in subsequent experiments. We next isolated cilia from wild-type or dominant-negative mutant-injected embryos and analyzed the average length of isolated cilia. Indeed, ciliary length was shorter with GJA1 dysfunction (Fig 2C). In particular, ciliary length was significantly decreased in each dominant-negative mutant-injected embryo (Fig 2D). These data indicate that GJA1 may play a role during ciliogenesis, especially ciliary axoneme assembly.

3. Morpholino-mediated knockdown of GJA1 disrupts the normal ciliogenesis in *Xenopus*.

Next, we sought to further confirm the necessity of GJA1 in ciliogenesis by depleting the proteins using an antisense morpholino oligo (MO). To test whether antisense MO-mediated knockdown also shows similar phenotypes to that of dominant-negative mutants, we designed the antisense MO to block translation by binding to the transcription start site. Antisense MO injection effectively reduced the expression level of wild-type GJA1 (Fig 3E, MO + wt-mRNA). In contrast, the translation of mismatch mRNA, which was modified to be mismatched with MO, was not affected as strongly as wild-type GJA1 mRNA by co-injection of GJA1-MO (Fig 3E, MO + mis-mRNA). Consistent to the mutant-based approaches, the cilia in GJA1-MO-injected embryos (morphants) were severely

malformed compared to those of control embryos (Fig 3A). Basal bodies were not severely affected by MO injection (Fig 3A, green). These data demonstrate that GJA1 may have critical functions in cilia formation following the basal body docking process. Moreover, the MO-mediated knockdown of GJA1 resulted in a smaller number of multi-ciliated cells in *Xenopus* embryonic epithelial tissues (Fig 3B middle panel, 3C). Co-injection of mature wild-type GJA1 mRNA with GJA1-MO effectively rescued the ciliary defects (Fig 3B right panel, 3C). We also co-injected each dominant-negative mRNA of GJA1 with GJA1-MO. However, dominant-negative mutants failed to reverse the ciliary defects seen in the GJA1 morphants (Fig 3D). Overall, these data indicate that GJA1 has previously unidentified functions for ciliary axoneme formation in multi-ciliated cells.

4. GJA1 function is necessary for GRP cilium formation and left-right asymmetry development.

Motile cilia are not only involved in mucus clearance in the muco-ciliary epithelium, but are also critical for determining left-right asymmetry during early embryonic development. Embryonic nodal cilium generates leftward flow, and this flow initiates the left LPM specification. In *Xenopus*, GRP (Gastrocoel roof plate) is known to possess nodal cilium, and this mono-, motile nodal cilium is necessary for left-right asymmetry formation [31, 32]. Therefore, we next determined if GJA1 is also necessary for GRP cilium formation. GJA1-MO was injected into the two dorsal-vegetal cells at 4-cell stage embryos to target GRP tissues. Indeed, GJA1 morphants displayed abnormally shortened nodal cilium in GRP, compared to those of control embryos (Fig 4A, 4B). Next, we assessed left-right asymmetry by observing heart development in later embryonic stages. In the ventral view, the truncus arteriosus of the control *Xenopus* embryonic heart was placed to the left of the embryos by looping of the primitive heart tube. Interestingly, we observed that approximately 30% of morphant embryos developed *situs inversus* (reversed organs) (Fig 4C, 4D). Furthermore, expression of the left LPM-specific marker, PITX2, was abnormal in GJA1-morphant embryos. (Fig 4E, 4F). These data demonstrate that GJA1 is also involved in motile nodal cilium formation at GRP in *Xenopus*.

5. siRNA-mediated knockdown of GJA1 disrupts primary ciliogenesis in human RPE1 cells.

Because the knockdown of GJA1 expression caused severe defects in the motile cilia of *Xenopus* epithelial tissues, we next examined the functions of GJA1 in primary ciliogenesis in human cells. We first observed the localization of GJA1 in human RPE1 cells by performing immunofluorescence analysis. As previously shown, GJA1 protein was localized to the gap junction at the cell periphery (Fig 5A, yellow square). Unexpectedly, we were not able to observe ciliary localization of GJA1 in the primary cilium. However, GJA1 signals accumulated in pericentriolar regions, where the primary cilium stemmed from (Fig 5A, white arrow). We speculated that GJA1 plays a role in primary cilium formation by affecting the PCM, which has been shown to be involved in cilia formation [33]. Furthermore, we depleted GJA1 in human RPE1 cells by siRNA transfection; this depletion was confirmed by immunoblotting (Fig 5C). Then, we observed primary cilium formation after inducing ciliogenesis in low-serum starvation conditions. We first confirmed that low-serum starvation effectively initiated cilia formation in human RPE1 cells (Fig S1A, S1B). Indeed, GJA1 depletion significantly disrupted cilia formation in RPE1 cells compared to control cells. Also, co-transfection of GJA1 cDNA plasmid with GJA1 siRNA partially rescued the siRNA phenotypes (Fig 5B, 5D). Interestingly, acetylated microtubules in the pericentriolar region were noticeably reduced in GJA1-depleted cells.

Next, we examined the subcellular localization of several key proteins that are known to be critical for ciliogenesis under GJA1-depleted conditions. Immunofluorescence staining of endogenous Arl13b, BBS4, CP110, IFT20, IFT88, and TTBK2, which are well-known PCM or ciliary markers, was performed. BBS4 and CP110 showed abnormal distribution in GJA1 siRNA-transfected cells, and there were no significant differences in the expression of other proteins, such as IFT20 and TTBK2 (Fig S2A, S2B). During cell cycle progression, CP110 is localized to the cap of mother and daughter centrioles and inhibits ciliary axoneme elongation. For proper primary cilium formation, CP110 must be removed from the cap of the mother centriole to initiate elongation of the ciliary axoneme [34, 35]. In addition, BBS4, which is a component of the BBSome complex, is localized around PCM and is

known to interact with PCM-1, dynein, and IFT during the delivery of ciliary building blocks to ciliary axonemes (Fig 6A) [36, 37]. Interestingly, we frequently observed two CP110 spots in both mother and daughter centrioles in siRNA-transfected RPE1 cells (Fig 6C, 6D). In addition, BBS4 was delocalized from the PCM, cilium, or basal bodies and exhibited distinct distribution as cytosolic puncta (Fig 6B), with non-ciliogenesis phenotypes. Although the mechanism of CP110 during *Xenopus* ciliogenesis has yet to be determined, CP110 phenotypes were similar to the GJA1 loss-of-function in RPE1 cells and were also observed in *Xenopus* epithelial multi-ciliated cells. GJA1-depleted embryos showed higher levels of CP110 signals compared with wild-type embryos (Fig S3). These data suggest that GJA1 is critical for primary cilium formation and may function in the cytoplasmic assembly of ciliary components around the PCM.

6. Rab11 interacts with GJA1, and knockdown of GJA1 interrupts Rab11 trafficking to basal bodies during ciliogenesis.

To identify the putative binding and functional partners of GJA1, we performed GJA1 immunoprecipitation and mass spectrometry (IP-MS). Then, we performed GO term analysis with 232 detected proteins and identified 2 major clusters of interest; regulation of calcium and ciliogenesis (Fig S4A, Table S1). A recent study revealed that the gap junction, especially GJA1, mediates the intracellular Ca^{2+} wave and regulates the maintenance of ependymal motile cilia through the Wnt-GJA1-Ca^{2+} axis [20]. Therefore, we examined if GJA1 depletion compromises cilia formation by affecting intracellular Ca^{2+} concentration in RPE1 cells. GJA1 depletion or overexpression showed similar Ca^{2+} concentrations at resting state and slightly affected Ca^{2+} entry, in comparison to RPE1 control cells (Fig S5A, S5B). However, the differences in Ca^{2+} entry were not as significant as that in previously reported research. Then, we next focused on the other cluster of ciliogenesis. Among dozens of interacting ciliary proteins, we selected Rab8 and Rab11 as candidates (Fig S4A). Both Rab8 and Rab11 have already been reported to be involved in ciliogenesis [25, 26, 37, 38]. Rab8 is localized in the primary cilium and regulates ciliary membrane extension [37, 38]. Previous research

has also shown that Rab8 interacts with CP110 and BBS4 [34, 35, 37]. Rab11 is enriched at the basal part of the primary cilium and recruits Rab8 to the basal body by interacting with Rabin8 [26, 38].

We first confirmed the interaction between GJA1 and Rab8 or Rab11 by performing co-immunoprecipitation, followed by the western blot assay. Consistent with the IP-MS data, GJA1 was successfully immunoprecipitated with Rab8a (Fig S6A) or Rab11a (Fig 7A), whereas the rabbit IgG negative control did not show any signals. Next, we confirmed the localization of GJA1 and Rab11 during ciliogenesis. As expected, GJA1 and Rab11 were co-localized in the PCM and acetylated tubulin network. In particular, GJA1 surrounded the Rab11 cluster, which was accumulated around the basal bodies. Furthermore, we observed decreased protein levels of Rab8a (Fig S6B) or Rab11 (Fig 7E) in GJA1-depleted RPE1 cells. Additionally, the accumulated localization of Rab11 at the base of the primary cilium disappeared upon GJA1 depletion, and these phenotypes were partially rescued with GJA1-cloned plasmid co-transfected cells (Fig 7C, F). We further confirmed the presence of Rab11-positive ciliary vesicles using structured illumination microscopy (SIM). At higher resolutions, SIM analysis showed that Rab11-positive vesicles encircled the base of the ciliary axoneme (Fig 7D). In contrast, GJA1-depleted cells showed scattered Rab11 signals. Overall, these data suggest that GJA1 controls the trafficking of Rab11-positive vesicles to the base of cilia during ciliogenesis.

Discussion

The gap junction complex is well-known to form a channel for mediating cell-to-cell communication. Gap junction-mediated cell-to-cell communication is indispensable for normal embryonic development, and the disruption of components of the gap junction complex causes embryonic lethality and various phenotypes in multiple organs [39-43]. For example, the mutation in GJA1, which is a major component of the gap junction complex, is known to cause a congenital disorder, ODDD, in humans [10]. However, recent studies strongly suggested that GJA1 possesses channel-independent functions to control cellular migration and polarity via regulating cytoskeletons, such as

actin filaments and microtubules, in various cell types, including cancer cells, neuronal progenitors, and cardiac neural crest cells [17, 19, 44, 45]. It has been suggested that the non-channel function of GJA1 may explain the complex disease phenotypes caused by GJA1 mutations in mice and humans [42, 46, 47].

While we were pursuing the molecular mechanism of GJA1 in ciliogenesis, Zhang et al published a paper arguing that GJA1 functions in maintenance of ependymal motile cilia in zebrafish spinal cord and also in mouse models (20). In this publication, Zhang et al. argued that GJA1 is a mediator of the calcium wave and signaling in Wnt-PLC-IP3 cascade to maintain the motile cilia.

In this study, we have confirmed the GJA1 localization in PCM and ciliary axonemes for the first time, suggesting the direct function of GJA1 in ciliogenesis. Also, we have confirmed that GJA1 depletion specifically affected CP110 removal from the mother centrioles and caused strong delocalization of BBS4 from the PCM and basal bodies, while several other key ciliary and PCM molecules, such as Arl13b, IFT20, IFT88, TTBK2, were not affected. These data suggest that GJA1 may possess very specific functions in general ciliogenesis in addition to functioning as a mediator of the calcium wave for the maintenance of motile cilia. Also, by performing IP/MS, we have found that Rab11 as an interaction partner which can explain how GJA1 may control the removal of CP110 from the mother centriole for the ciliogenesis.

Previous studies have investigated the possible function of gap junction proteins, such as GJB2 (gap junction protein beta 2; CX26), GJA1 (CX43), and GJA7 (gap junction protein alpha 7; CX43.4), in determining left-right asymmetry. Most studies on the function of gap junction proteins in determining laterality have indicated that the channel function is critical in mediating leftward signals, which are driven by nodal cilia [48-50]. For example, GJB2 has been shown to be a key gap junction protein involved in determining left-right asymmetry, whereas the GRP cilium is largely unaffected by GJB2 depletion [48].

Our study supports the finding that GJA1, a major connexin CX43, is critical for cilia formation in both motile and primary cilia. The GJA1 cytosolic domain contains a microtubule-binding motif that

is necessary for trafficking to the gap junction complex. Furthermore, GJA1 seems to exhibit non-channel functions that mainly control cytoskeletons and give directional cues for the migrating cells [30, 44, 51].

Interestingly, cilia have also been shown to be necessary for the polarization of migrating cells and directional protrusion, such as lamellipodia [52, 53]. Given the complex loss-of-function phenotype of GJA1, it is a feasible hypothesis that some of the non-channel functions of GJA1 may be mediated by regulating cilia formation. GJA1 was localized to the PCM microtubules in human RPE1 cells, and GJA1 depletion resulted in reduced acetylated tubulin levels in PCM microtubules. PCM microtubules are known to be critical for the transport of ciliary building blocks to the basal bodies, the organizing center for cilia. Indeed, several PCM microtubules have been shown to be involved in cilia formation by organizing the PCM and associated protein transport [54-56]. These data suggest a possible mechanism of GJA1-mediated ciliogenesis, in which GJA1 modulates the transportation of ciliary materials. Indeed, our data show that GJA1 interacted with Rab11 and controlled the trafficking of Rab11-positive vesicles to the ciliary base (Fig S7).

An interesting discrepancy in our data was the differential localization of GJA1 in multi-cilia and primary cilia. GJA1 displayed two distinct localizations in multi-cilia: the basal bodies and axonemes. Interestingly, GJA1 was localized to the PCM regions in primary cilia-forming cells, but not in the basal bodies or axonemes. We believe this discrepancy may be due to functional and structural differences between motile cilia and non-motile primary cilia.

Finally, although we were not able to explain why GJA1 depletion caused strong delocalization of BBS4, this finding strongly supports more direct function of GJA1 in ciliogenesis in addition to the maintenance of ependymal cilia. Here, we provided critical evidence for GJA1 functions and mechanisms in cilia formation and ciliopathy phenotypes. Further studies to examine the functions of GJA1 in transporting ciliary building blocks may elucidate the molecular function of GJA1 in cilia formation.

Materials and Methods

1. *Xenopus laevis* rearing

Ovulation was induced in adult female *Xenopus laevis* by the injection of human chorionic gonadotropin. Eggs were then fertilized *in vitro* and dejellied with 3% cysteine in a 1/3× MMR (Marc's Modified Ringers) (pH 7.8~7.9) solution. After fertilization, eggs were reared in 1/3× MMR.

1.1. Microinjection procedure

For microinjections, embryos were placed in 1% Ficoll in 1/3X MMR solution. To target the epithelial tissue or GRP tissue in *Xenopus* embryos, we injected into the ventral-animal region (epithelial tissue) or dorsal-vegetal region (GRP tissue), respectively, of the blastomeres at 2- or 4-cell stages [57] using a Picospritzer III microinjector (Parker, NH, USA). The injected eggs were grown in 1/3× MMR with antibiotics (Gentamycin). We injected MO at 70 ng per embryo, and wild-type or dominant-negative mutant mRNAs were injected in various amounts.

1.2. Morpholino

We designed translation-blocking antisense MO for GJA1, based on the sequence from the Xenbase database. Morpholino is manufactured by Gene Tools (OR, USA) (GJA1-MO: 5'-TTCCTAAGGCACTCCAGTCACCCAT-3').

1.3. Fixation

To analyze the development of epithelial cilia, we fixed embryos at stage 26~30 using MEMFA (2× MEM salts and 7.5% formaldehyde) or DENT's fixative solution (20% DMSO in Methanol).

1.4. Cilia isolation

Cilia isolation was performed using a modified calcium shock method, as previously described [58], Briefly, deciliation solution (20 mM Tris-HCl [pH 7.5], 50 mM NaCl, 10 mM $CaCl_2$, 1 mM EDTA, 7 mM β-mercaptoethanol, and 0.1% Triton X-100) was added to the embryos, and the test tube was gently inverted for 30 seconds. To remove the cellular debris, samples were centrifuged at 1,500 g for 2 min, and the supernatant was transferred to new e-tubes. Cilia in the supernatant were pelleted by centrifugation at 12,000 g for 5 min. After discarding the supernatant, MEMFA or DENT's fixative solution was added immediately to fix the cilia pellet.

1.5. *In situ* hybridization

Whole-mount *in situ* hybridization (WISH) was performed with a modified method, as previously described [59].

1.6. GRP tissue explant preparation

GRP tissue explants were prepared as previously described [32]. To image GRP nodal cilia, stage 17 embryos were fixed and cut in the anterior head before immunofluorescence staining. Then, GRP tissue explants were mounted on the cover glass.

2. Human RPE1 cell culture

Human RPE1 cells were cultured under standard mammalian cell conditions with 10% FBS (Gibco, ThermoFisher Scientific, MA, USA) and 1% antibiotics in DMEM/F12 (1:1) media (Gibco).

2.1. Transfection

For GJA1 siRNA knockdown experiments, RPE1 cells were transfected with siRNA (Genolution, Seoul, Republic of Korea, sense, 5'-GUUCAAGUACGGUAUUGAAUU-3') using jetPRIME® transfection reagent (Polyplus, NY, USA). Exogenous plasmid DNA was transfected using Transporter™ 5 transfection reagent (Polysciences, PA, USA). Co-transfection of siRNA with plasmid DNA was performed using jetPRIME® transfection reagent. All transfections were performed in Opti-MEM® conditions (Gibco). The final concentration of siRNA was 70 nM. Transfected cells were incubated for a total of 48 hours, including the serum starvation step.

2.2. Ciliation and serum starvation

For the primary ciliation of RPE1, cells were incubated in serum-free DMEM/F12 media (Gibco) for at least 24 hours.

2.3. Fixation

To analyze primary cilium development, RPE1 cells were fixed in PFA (4% formaldehyde in 1X PBS) fixative solution after ciliation.

2.4. Intracellular Ca^{2+} entry imaging

For intracellular Ca^{2+} imaging, GJA1 siRNA- or plasmid DNA-transfected RPE1 cells were cultured on fibronectin (Sigma Aldrich, MO, USA)-coated cover glasses. Cells were loaded with 2 μM Fura-2/AM (Invitrogen, ThermoFisher Scientific, MA, USA). Ratiometric Ca^{2+} imaging was performed at 340 and 380 nm in 0 or 2 mM Ca^{2+} Ringer's solution with an IX81 microscope (Olympus, Tokyo, Japan) at room temperature. Images were processed with Metamorph and analyzed with Igor P. Ca^{2+} peaks were calculated by determining the maximum of each trace upon application of 0.5 μM thapsigargin (Santa Cruz, TX, USA) and Ca^{2+}, and baseline values prior to application were

subtracted.

3. Cloning and plasmid information

The full-length sequences of *Xenopus laevis* GJA1, human GJA1, Rab8a, and Rab11a genes were obtained from the Xenbase database or Pubmed. Total *Xenopus laevis* RNA was purified from stage 35~36 embryos, and total human RNA was purified from RPE1 cells. Next, we reverse-transcribed cDNA with random primer mix (NEB, MA, USA) and GoScript™ Reverse Transcriptase (Promega, WI, USA). We designed the primer pairs with a restriction enzyme site for cloning (Table 1). For the rescue experiments, point mutations were generated in the MO- or siRNA-binding sequences of GJA1 cDNA. We designed the primer pairs for silence-point mutation (Table 1). Amplified *Xenopus* GJA1, human GJA1, Rab8a, and Rab11a PCR products were cloned into the CS108 or pcDNA3.0 vectors and fused to Flag- or HA-tag sequences at the C-terminus of the CDS. Dominant-negative forms of GJA1 constructs were generated based on cloned *Xenopus laevis* wild-type GJA1-Flag plasmid with deletion or point mutation primer pairs (Table 1). After PCR amplification using the primers, the DpnI enzyme was treated and transformed into DH5α *E. coli*. Wild-type or dominant-negative GJA1 mRNAs were transcribed by using mMESSAGE mMACHINE™ SP6 transcription Kit (Invitrogen), and the antisense probe of wild-type GJA1 using T7 RNA polymerase (Promega) with dig-dNTP mix (Roche, Basel, Switzerland) from the cloned plasmid.

Table 1. Primer information

Primer Name	**Primer Sequences (5' – 3')**
SalI-xlGJA1-Forward	aatgtcgacATGGGTGACTGGAGTGCCTTAGG
XbaI-xlGJA1-Backward	aattctagaGATCTCTAAATCATCAGGTCGTGGTCT
SalI-hGJA1-Forward	aatgtcgacATGGGTGACTGGAGCGCCT

XbaI-hGJA1-Backward	aattctagaGATCTCCAGGTCATCAGGCCG
point mut-xlGJA1-Forward	CGACATGGGGGATTGGAGCGCATTGGGAAGACTT
point mut-xlGJA1-Backward	AGTCTTCCCAATGCGCTCCAATCCCCCATGTCGA
point mut-hGJA1-Forward	TGAGATAAAGAAATTTAAATATGGAATAGAGGAGCA TGGTAAGGTGAAA
point mut-hGJA1-Backward	CTTACCATGCTCCTCTATTCCATATTTAAATTTCTTTA TCTCAATCTGC
SalI-hRab8a-Forward	aatgtcgacATGGCGAAGACCTACGATTACCTG
XbaI-hRab8a-Backward	aattctagaCAGAAGAACACATCGGAAAAAGCTG
SalI-hRab11a-Forward	aatgtcgacATGGGCACCCGCGACG
XbaI-hRab11a-Backward	aattctagaGATGTTCTGACAGCACTGCACCTT
xlGJA1-T154A-Forward	AAAGTCAAGATGCGAGGTGGACTGCTTCGCGCCTA CATCATCAGCATTTTGTTTAAA
xlGJA1-T154A-Backward	TACTGATTTAAACAAAATGCTGATGATGTAGGCGCG AAGCAGTCCACCTCGCATCTT
xlGJA1-Δ130-136-Forward	ATGCACCTTAAACAATATGGCCTTGAAGAG
xlGJA1-Δ130-136-Backward	CTCTTCAAGGCCATATTGTTTAAGGTGCAT
xlGJA1-Δ234-243-Forward	TTCTATGTCACCTACAAAGACCCATTTTCT
xlGJA1-Δ234-243-Backward	AGAAAATGGGTCTTTGTAGGTGACATAGAA

4. Immunofluorescence

Embryos were fixed with MEMFA or DENT's fixative solution overnight at 4°C, and RPE1 cells were fixed with 4% PFA solution for 20 min at room temperature. Fixed embryos or RPE1 cells were incubated in blocking solution (10% FBS, 2% DMSO in 1× TBS with 0.1% Triton X-100) for 30 min at room temperature to block non-specific binding. Immunostaining was performed with the following antibodies at 1:50~500 dilution in blocking solution for 1~2 hours at room temperature: anti-DDDD-

K (Abcam, Cambridge, UK), anti-GFP (Abcam), anti-RFP (Abcam), anti-acetylated tubulin (Sigma Aldrich), anti-γ-tubulin (Abcam), anti-MyHC (DSHB, IA, USA), anti-CP110 (Proteintech, IL, USA), anti-BBS4 (Proteintech), anti-Rab8a (CST, MA, USA), anti-Rab11 (CST), and anti-GJA1 (ThermoFisher Scientific). Fluorescence labeling was performed using DAPI (1:10,000, ThermoFisher Scientific) and Alexa Fluor 488-, 555-, and 633-conjugated secondary antibodies (1:300, Invitrogen).

5. Immunoblotting

Xenopus or human RPE1 immunoblotting samples were prepared with modified lysis buffer (TBS, 1% Triton X-100, 10% Glycerol with protease inhibitor). After removing fat and cellular debris, SDS sample buffer with DTT was added. Samples were loaded on SDS-PAGE gels and transferred to polyvinylidene fluoride membranes (Merck Millipore, MA, USA). Membranes were incubated in blocking solution (TBS, 0.05% Tween-20 with non-fat powdered milk) for 30 min at room temperature to block non-specific binding. Immunoblotting was performed with the following antibodies at 1:2500~3000 dilution for either 1 hour at room temperature or overnight at 4°C: anti-DDDD-K (Abcam), anti-α-actin (ThermoFisher Scientific), anti-α-tubulin (Abcam), anti-GJA1 (ThermoFisher Scientific), anti-HA (Santa Cruz), anti-Rab8a (CST), and anti-Rab11 (CST). Secondary labeling was performed using horseradish peroxidase-conjugated, anti-mouse or anti-rabbit IgG antibodies (ThermoFisher Scientific; 1:3000) for 1 hour at room temperature. Chemiluminescence was performed with Enhanced Chemiluminescence substrate (ThermoFisher Scientific) and imaged with iBright imaging systems (FL1000, ThermoFisher Scientific).

6. Immunoprecipitation and mass spectrometry

For immunoprecipitation of GJA1, we produced anti-GJA1 antibody-conjugated paramagnetic beads. Anti-GJA1 antibody (ThermoFisher Scientific) or rabbit normal serum (Abclon, Seoul, Republic of

Korea) was cross-linked with Protein G Mag Sepharose beads (GE Healthcare, IL, USA), according to the manufacturer's instructions. Human RPE1 lysate was prepared with immunoblotting lysis buffer and incubated with GJA1- or rabbit serum-conjugated beads overnight at 4°C. The beads were washed with lysis buffer and eluted with low-pH elution buffer (0.1 M glycine-HCl, pH 2.9). Next, eluted samples were concentrated by Amicon® Ultra (Merck Millipore), and SDS sample buffer and DTT were added. For mass spectrometry, protein samples were separated on an SDS-PAGE Tris-glycine 12% gel. The gel was stained with Coomassie brilliant blue G-250 overnight, after which it was destained with destaining solution (10% ethanol/2% orthophosphoric acid). Gel pieces were destained in 1:1 methanol:50 mM ammonium bicarbonate, and destained gels were dehydrated by 100% acetonitrile and then incubated in 25 mM DTT in 50 mM ammonium bicarbonate for 20 min at 56°C. After removing DTT solution, the samples were alkylated in 25 mM iodoacetamide in 100 mM ammonium bicarbonate solution. The iodoacetamide solution was removed and then dehydrated with 100% acetonitrile. Approximately 0.25 μg MS-grade trypsin protease was added to each sample, along with 100μL of a 50 mM ammonium bicarbonate/10% acetonitrile solution. Protein samples were then digested overnight at 37°C. After digestion, 100 μL of 50% acetonitrile/0.1% formic acid solution was added to the trypsin solution for 3 min at 56°C. The extraction solution (99.9% acetonitrile/0.1% formic acid; 100 μL) was added to each sample for 3 min at 56°. Collected peptides were dried and dissolved with 20 μL of the 0.1% TFA solution and purified with C18 tips. Eluted samples were dried completely in a vacuum concentrator and resuspended with 20 μL of the 0.1% formic acid solution. The samples were analyzed by a high-resolution mass spectrometer (Orbitrap Fusion Lumos, ThermoFisher Scientific).

7. Data availability

All data generated or analyzed during this study are included in the manuscript and supporting files. Source data file is provided for statistical figure. The dataset obtained from the GJA1 IP/MS experiment can be accessed in Dryad (https://doi.org/10.5061/dryad.tht76hdxt) (Fig. S4A, Table S1).

8. Microscopy

Images were captured using confocal microscopy (LSM780, LSM880, both Zeiss, Oberkochen, Germany), stereo microscopy (SZX16, Olympus), and SIM (ELYRA S.1, Zeiss). Images were performed using ZEN software for merging, 3D images, and SIM processing.

9. Image analysis, Statistical analysis

Quantitative analyses of the average ciliary length and number of multi-ciliated or RPE1 cells were performed with ZEN and ImageJ programs. Statistical analyses were produced using Graphpad Prism 8. P values were calculated using the two-tailed t-test or one-way ANOVA, and data were indicated as mean ± S.D.

Acknowledgements

The authors thanks to Dr. M. Ko and Dr. S. H. Park for critical discussions.

This work was supported by Korea National Research Foundation (2018R1A2B2007545, 2019M3E5D5067273) and Institute for Basic Science (IBS-R001-D1).

Competing interests

The authors declare no competing interests.

References

1. Goodenough, D.A., J.A. Goliger, and D.L. Paul, *Connexins, connexons, and intercellular*

communication. Annu Rev Biochem, 1996. **65**: p. 475-502.

2. Goodenough, D.A. and D.L. Paul, *Gap junctions.* Cold Spring Harb Perspect Biol, 2009. **1**(1): p. a002576.

3. Aasen, T., *Connexins: junctional and non-junctional modulators of proliferation.* Cell Tissue Res, 2015. **360**(3): p. 685-99.

4. El-Sabban, M.E., L.F. Abi-Mosleh, and R.S. Talhouk, *Developmental regulation of gap junctions and their role in mammary epithelial cell differentiation.* J Mammary Gland Biol Neoplasia, 2003. **8**(4): p. 463-73.

5. Vinken, M., et al., *Connexins and their channels in cell growth and cell death.* Cell Signal, 2006. **18**(5): p. 592-600.

6. Bosco, D., J.A. Haefliger, and P. Meda, *Connexins: key mediators of endocrine function.* Physiol Rev, 2011. **91**(4): p. 1393-445.

7. Söhl, G. and K. Willecke, *Gap junctions and the connexin protein family.* Cardiovasc Res, 2004. **62**(2): p. 228-32.

8. Beyer, E.C., D.L. Paul, and D.A. Goodenough, *Connexin43: a protein from rat heart homologous to a gap junction protein from liver.* J Cell Biol, 1987. **105**(6 Pt 1): p. 2621-9.

9. Boyadjiev, S.A., et al., *Linkage analysis narrows the critical region for oculodentodigital dysplasia to chromosome 6q22-q23.* Genomics, 1999. **58**(1): p. 34-40.

10. Paznekas, W.A., et al., *Connexin 43 (GJA1) mutations cause the pleiotropic phenotype of oculodentodigital dysplasia.* Am J Hum Genet, 2003. **72**(2): p. 408-18.

11. Oyamada, M., Y. Oyamada, and T. Takamatsu, *Regulation of connexin expression.* Biochim Biophys Acta, 2005. **1719**(1-2): p. 6-23.

12. Evans, W.H. and P.E. Martin, *Gap junctions: structure and function (Review).* Mol Membr Biol, 2002. **19**(2): p. 121-36.

13. Ruangvoravat, C.P. and C.W. Lo, *Connexin 43 expression in the mouse embryo: localization of transcripts within developmentally significant domains.* Dev Dyn, 1992. **194**(4): p. 261-81.

14. Willecke, K., et al., *Structural and functional diversity of connexin genes in the mouse and*

human genome. Biol Chem, 2002. **383**(5): p. 725-37.

15. Beyer, E.C., D.L. Paul, and D.A. Goodenough, *Connexin family of gap junction proteins.* J Membr Biol, 1990. **116**(3): p. 187-94.

16. Leithe, E., M. Mesnil, and T. Aasen, *The connexin 43 C-terminus: A tail of many tales.* Biochim Biophys Acta, 2018. **1860**(1): p. 48-64.

17. Matsuuchi, L. and C.C. Naus, *Gap junction proteins on the move: connexins, the cytoskeleton and migration.* Biochim Biophys Acta, 2013. **1828**(1): p. 94-108.

18. Kameritsch, P., K. Pogoda, and U. Pohl, *Channel-independent influence of connexin 43 on cell migration.* Biochim Biophys Acta, 2012. **1818**(8): p. 1993-2001.

19. Rhee, D.Y., et al., *Connexin 43 regulates epicardial cell polarity and migration in coronary vascular development.* Development, 2009. **136**(18): p. 3185-93.

20. Zhang, J., et al., *Wnt-PLC-IP3-Connexin-Ca(2+) axis maintains ependymal motile cilia in zebrafish spinal cord.* Nat Commun, 2020. **11**(1): p. 1860.

21. Gerdes, J.M., E.E. Davis, and N. Katsanis, *The vertebrate primary cilium in development, homeostasis, and disease.* Cell, 2009. **137**(1): p. 32-45.

22. Malicki, J.J. and C.A. Johnson, *The Cilium: Cellular Antenna and Central Processing Unit.* Trends Cell Biol, 2017. **27**(2): p. 126-140.

23. Waters, A.M. and P.L. Beales, *Ciliopathies: an expanding disease spectrum.* Pediatr Nephrol, 2011. **26**(7): p. 1039-56.

24. Fliegauf, M., T. Benzing, and H. Omran, *When cilia go bad: cilia defects and ciliopathies.* Nat Rev Mol Cell Biol, 2007. **8**(11): p. 880-93.

25. Knodler, A., et al., *Coordination of Rab8 and Rab11 in primary ciliogenesis.* Proc Natl Acad Sci U S A, 2010. **107**(14): p. 6346-51.

26. Westlake, C.J., et al., *Primary cilia membrane assembly is initiated by Rab11 and transport protein particle II (TRAPPII) complex-dependent trafficking of Rabin8 to the centrosome.* Proc Natl Acad Sci U S A, 2011. **108**(7): p. 2759-64.

27. James-Zorn, C., et al., *Xenbase: expansion and updates of the Xenopus model organism*

database. Nucleic Acids Res, 2013. **41**(Database issue): p. D865-70.

28. Beahm, D.L., et al., *Mutation of a conserved threonine in the third transmembrane helix of alpha- and beta-connexins creates a dominant-negative closed gap junction channel.* J Biol Chem, 2006. **281**(12): p. 7994-8009.

29. Wang, M., et al., *Connexin43 with a cytoplasmic loop deletion inhibits the function of several connexins.* Biochem Biophys Res Commun, 2005. **333**(4): p. 1185-93.

30. Giepmans, B.N., et al., *Gap junction protein connexin-43 interacts directly with microtubules.* Curr Biol, 2001. **11**(17): p. 1364-8.

31. Schweickert, A., et al., *Cilia-driven leftward flow determines laterality in Xenopus.* Curr Biol, 2007. **17**(1): p. 60-6.

32. Blum, M., et al., *Xenopus, an ideal model system to study vertebrate left-right asymmetry.* Dev Dyn, 2009. **238**(6): p. 1215-25.

33. Moser, J.J., et al., *The PCM-basal body/primary cilium coalition.* Semin Cell Dev Biol, 2010. **21**(2): p. 148-55.

34. Tsang, W.Y., et al., *CP110 suppresses primary cilia formation through its interaction with CEP290, a protein deficient in human ciliary disease.* Dev Cell, 2008. **15**(2): p. 187-97.

35. Tsang, W.Y. and B.D. Dynlacht, *CP110 and its network of partners coordinately regulate cilia assembly.* Cilia, 2013. **2**(1): p. 9.

36. Uytingco, C.R., et al., *BBS4 is required for intraflagellar transport coordination and basal body number in mammalian olfactory cilia.* J Cell Sci, 2019. **132**(5).

37. Nachury, M.V., et al., *A core complex of BBS proteins cooperates with the GTPase Rab8 to promote ciliary membrane biogenesis.* Cell, 2007. **129**(6): p. 1201-13.

38. Blacque, O.E., N. Scheidel, and S. Kuhns, *Rab GTPases in cilium formation and function.* Small GTPases, 2018. **9**(1-2): p. 76-94.

39. Meşe, G., G. Richard, and T.W. White, *Gap junctions: basic structure and function.* J Invest Dermatol, 2007. **127**(11): p. 2516-24.

40. Laird, D.W., *The gap junction proteome and its relationship to disease.* Trends Cell Biol,

2010. **20**(2): p. 92-101.

41. Dobrowolski, R. and K. Willecke, *Connexin-caused genetic diseases and corresponding mouse models.* Antioxid Redox Signal, 2009. **11**(2): p. 283-95.

42. Pfenniger, A., A. Wohlwend, and B.R. Kwak, *Mutations in connexin genes and disease.* Eur J Clin Invest, 2011. **41**(1): p. 103-16.

43. Srinivas, M., V.K. Verselis, and T.W. White, *Human diseases associated with connexin mutations.* Biochim Biophys Acta Biomembr, 2018. **1860**(1): p. 192-201.

44. Francis, R., et al., *Connexin43 modulates cell polarity and directional cell migration by regulating microtubule dynamics.* PLoS One, 2011. **6**(10): p. e26379.

45. Crespin, S., et al., *The carboxy-terminal tail of connexin43 gap junction protein is sufficient to mediate cytoskeleton changes in human glioma cells.* J Cell Biochem, 2010. **110**(3): p. 589-97.

46. Laird, D.W., *Syndromic and non-syndromic disease-linked Cx43 mutations.* FEBS Lett, 2014. **588**(8): p. 1339-48.

47. Laird, D.W., *Closing the gap on autosomal dominant connexin-26 and connexin-43 mutants linked to human disease.* J Biol Chem, 2008. **283**(6): p. 2997-3001.

48. Beyer, T., et al., *Connexin26-mediated transfer of laterality cues in Xenopus.* Biol Open, 2012. **1**(5): p. 473-81.

49. Levin, M. and M. Mercola, *Gap junctions are involved in the early generation of left-right asymmetry.* Dev Biol, 1998. **203**(1): p. 90-105.

50. Hatler, J.M., J.J. Essner, and R.G. Johnson, *A gap junction connexin is required in the vertebrate left-right organizer.* Dev Biol, 2009. **336**(2): p. 183-91.

51. Fu, Y., et al., *Cx43 Isoform GJA1-20k Promotes Microtubule Dependent Mitochondrial Transport.* Front Physiol, 2017. **8**: p. 905.

52. Veland, I.R., L. Lindbaek, and S.T. Christensen, *Linking the Primary Cilium to Cell Migration in Tissue Repair and Brain Development.* Bioscience, 2014. **64**(12): p. 1115-1125.

53. Schneider, L., et al., *Directional cell migration and chemotaxis in wound healing response to*

PDGF-AA are coordinated by the primary cilium in fibroblasts. Cell Physiol Biochem, 2010. **25**(2-3): p. 279-92.

54. Kim, J., S.R. Krishnaswami, and J.G. Gleeson, *CEP290 interacts with the centriolar satellite component PCM-1 and is required for Rab8 localization to the primary cilium.* Hum Mol Genet, 2008. **17**(23): p. 3796-805.

55. Kim, K., K. Lee, and K. Rhee, *CEP90 is required for the assembly and centrosomal accumulation of centriolar satellites, which is essential for primary cilia formation.* PLoS One, 2012. **7**(10): p. e48196.

56. Lopes, C.A., et al., *Centriolar satellites are assembly points for proteins implicated in human ciliopathies, including oral-facial-digital syndrome 1.* J Cell Sci, 2011. **124**(Pt 4): p. 600-12.

57. Hubrecht-Laboratorium (Embryologisch Instituut), P.D. Nieuwkoop, and J. Faber, *Normal table of Xenopus laevis (Daudin). A systematical and chronological survey of the development from the fertilized egg till the end of metamorphosis*. 2. ed. 1967, Amsterdam,: North-Holland Pub. Co. 260 p. with illus. with 10 fold. l.

58. Hastie, A.T., et al., *Isolation of cilia from porcine tracheal epithelium and extraction of dynein arms.* Cell Motil Cytoskeleton, 1986. **6**(1): p. 25-34.

59. Harland, R.M., *In situ hybridization: an improved whole-mount method for Xenopus embryos.* Methods Cell Biol, 1991. **36**: p. 685-95.

Figure Legends

Figure 1. GJA1 was localized to the ciliary axoneme in *Xenopus* multi-ciliated cells.

A. The schematic structure of gap junction channels and GJA1.

B, C. Immunofluorescence analysis of the localization of GJA1 in *Xenopus* epithelial multi-ciliated cells. *Xenopus* embryos were microinjected with GJA1 Flag-tagged mRNA, and the embryos were stained with antibodies against acetylated tubulin (Green) and Flag (Red). Scale bars: 10-µm

B', C'. X-Z projection images of panels **B, C.**

Figure 2. GJA1 dysfunction caused ciliary defects in *Xenopus* multi-ciliated cells.

A. The schematic image of dominant-negative mutants of GJA1. The T154A mutant contained the threonine (154)-to-alanine point mutation at transmembrane domain (TM) 3. The Δ130-136 mutant was a deletion mutant of the intracellular loop between TM 2 and 3. Δ234-243 was also a deletion mutant of the C-terminus of GJA1.

B. *Xenopus* embryos were injected with GJA1 dominant-negative mutant mRNAs and then immunostained. The ciliary axonemes were stained with acetylated tubulin antibody (Red). Basal bodies were visualized by microinjection of centrin-GFP (Green). Cellular membranes were labeled by membrane RFP and detected using an anti-RFP antibody (Blue). Scale bars: 10-µm.

C. GJA1 dominant-negative mutant-injected embryos were treated with cilia isolation buffer, and isolated cilia were labeled with the acetylated tubulin antibody (Red). Scale bars: 10-µm.

D. The average lengths of ciliary axonemes in panel **C** were plotted. Error bars represent mean ± s.d. (n=20 with 2 independent experiments, 10 values per experiment). P values were determined with the two-tailed t-test (P: ***=0.0004, ****<0.0001).

Figure 3. Morpholino-mediated knockdown of GJA1 caused the severe disruption of ciliogenesis in *Xenopus* multi-ciliated cells.

A. Microinjection of GJA1 antisense morpholino (MO) disrupted normal ciliary axoneme assembly. The ciliary axonemes were labeled with acetylated tubulin antibody (Red), and centrosome or basal bodies were stained with γ-tubulin antibody (Green). The membranes were labeled by microinjection of membrane RFP and detected by an anti-RFP antibody (Blue) at stage 30. Scale bars: 10-µm.

B. Low-magnification confocal images of *Xenopus* epithelial multi-ciliated cells. Multi-cilia bundles were stained with acetylated tubulin (Red), and membranes were labeled by microinjection of membrane-GFP and detected with an anti-GFP antibody (Green) at stage 30. Scale bars: 100-µm.

C. Statistical analysis of the number of multi-ciliated cells per unit area in panel **B.** Error bars represent mean ± s.d. (n=8 with 2 independent experiments, 4 values per experiment). P values were determined with the two-tailed t-test (P: **=0.0010, *=0.0152).

D. Wild-type (WT) or dominant-negative mutant Flag-tagged mRNAs were co-injected with GJA1-MO. Only WT GJA1 mRNA rescued the loss-of-function phenotype. Each GJA1 Flag-tagged protein was detected by the Flag antibody (Green). Ciliary axonemes (Red) and cell membranes (Blue) were visualized with the anti-acetylated antibody and anti-GFP antibody, respectively. Scale bars: 10-µm.

E. Wild-type (WT) or MO binding site silent mutant (mis) with Flag-tagged GJA1 protein was co-injected with GJA1-MO into embryos. Immunoblotting was performed with Flag antibody for exogenous GJA1 protein, with α-tubulin as the loading control.

Figure 4. GJA1 depletion disrupted GRP cilia formation and left-right asymmetry.

A. GJA1-MO was injected into the dorso-vegetal blastomeres to target GRP tissues. Nodal cilia, In the GRP was stained with an anti-acetylated tubulin antibody (Green), and the cell membrane was visualized by membrane-GFP, which was detected by an anti-GFP antibody (Red). Scale bars: 20-µm.

B. The average lengths of GRP ciliary axonemes were plotted. Error bars represent mean ± s.d. (n=100 with 3 independent experiments, 33~34 values per experiment). P values were determined with the two-tailed t-test (P: ****<0.0001).

C-D. GJA1 depletion reversed heart looping in *Xenopus* embryos. The embryonic hearts were visualized by immunostaining with an anti-myosin heavy chain antibody (lower panel). GJA1 morphants displayed reversed heart looping. Approximately 30% of MO-injected embryos displayed reversed heart looping (n indicated in graph, 2 independent experiments). Scale bars: 500-µm (Upper panel), 100-µm (Lower panel). TA; Truncus arteriosus, V; Ventricle.

E-F. Left LPM-specific marker, PITX2, expression was disrupted in GJA1 morphants (n indicated in graph, 2 independent experiments). Scale bars: 1-mm.

Figure 5. siRNA-mediated GJA1 depletion severely disrupted primary cilia formation in human RPE1 cells.

A. RPE1 cells were serum starved for 24 hr and labeled with anti-GJA1 antibody (Green), anti-acetylated tubulin antibody (Red), and DAPI (Blue). Scale bars: 20-µm (Left panel), 10-µm (Right panel).

B. siRNA-mediated knockdown of GJA1 inhibited primary cilia formation, and the ciliary defects were rescued by GJA1 transfection in human RPE1 cells. GJA1 was labeled with anti-GJA1 antibody (Red), and the primary cilium was stained with acetylated tubulin (Green). Scale bars: 10-µm.

C. siRNA transfection effectively depleted GJA1 levels in human RPE1 cells. Immunoblotting was

performed with an anti-GJA1 antibody and an anti-α-tubulin antibody as the loading control.

D. Statistical analysis of the percentage of ciliated cells in panel **B.** Error bars represent mean ± s.d. (n=8 with 2 independent experiments, 4 values per experiment, Total counted cell #: CTL=417, siRNA=242, Rescue=193). P values were determined with the two-tailed t-test (P: ****<0.0001, *=0.0136).

Figure 6. Knockdown of GJA1 resulted in the abnormal distribution of pericentriolar material (PCM) markers involved in ciliogenesis.

A. Cellular localization of PCM markers, CP110 and BBS4, during ciliogenesis.

B. RPE1 cells were transfected with GJA1 siRNA and immunostained with an anti-BBS4 antibody (Green) and an anti-acetylated tubulin antibody (Red). Scale bars: 20-μm.

C. RPE1 cells were transfected with GJA1 siRNA and immunostained with an anti-CP110 antibody (Green), anti-acetylated tubulin antibody (Red), and DAPI (Blue). Scale bars: 20-μm (Left panel), 5-μm (Right panel).

D. The percentage of CP110 dots per cell in panel **C.** Error bars represent mean ± s.d. (n=2 with 2 independent experiments, 1 value per experiment, Total counted cell #: CTL=24, siRNA=22). P values were determined with the two-tailed t-test (P: **=0.0059).

Figure 7. Knockdown of GJA1 disrupted Rab11 trafficking to the ciliary base.

A. HA-tagged Rab11 protein was immunoprecipitated by GJA1 antibody-conjugated beads, and immunoblotting was performed with anti-GJA1 and anti-HA antibodies.

B. RPE1 cells were serum starved for 24 hr and labeled with an anti-Rab11 antibody (Green), anti-GJA1 antibody (Red), anti-acetylated tubulin antibody (Blue), and DAPI (Grey). Scale bars: 5-µm.

C. siRNA-mediated knockdown of GJA1 inhibited Rab11 accumulation around the basal bodies, and GJA1 transfection rescued the phenotype in RPE1 cells. RPE1 cells were immunostained with an anti-Rab11 antibody (Green), anti-GJA1 antibody (Red), anti-acetylated tubulin antibody (Blue), and DAPI (Grey). Scale bars: 10-µm.

D. High-resolution images of Rab11 localization. RPE1 cells were labeled with an anti-Rab11 antibody (Green) and anti-acetylated tubulin antibody (Red). The images were obtained by structured illumination microscopy. Scale bars: 1-µm.

E. Rab11 and GJA1 expression levels were analyzed by immunoblotting with an anti-GJA1 antibody and anti-Rab11 antibody, respectively, in GJA1 siRNA-transfected RPE1 cells. Anti-actin antibody was used as the loading control.

F. Statistical analysis of Rab11 accumulation in panel **C.** Error bars represent mean ± s.d. (n=4 with 2 independent experiments, 2 values per experiment, Total counted cell #: CTL=194, siRNA=114, Rescue=108). P values were determined with the two-tailed t-test (P: **=0.0063, *=0.0447).

Figure 1

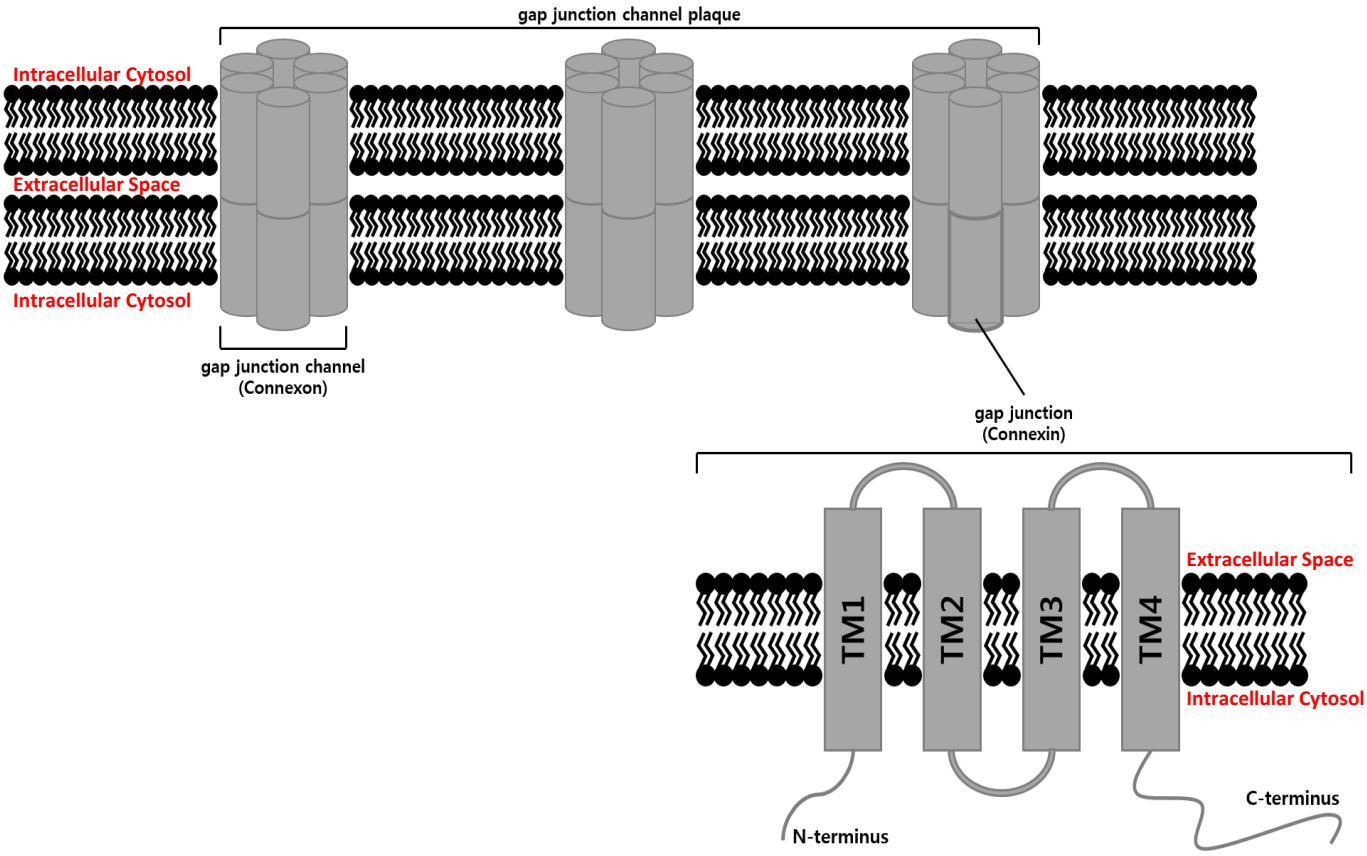

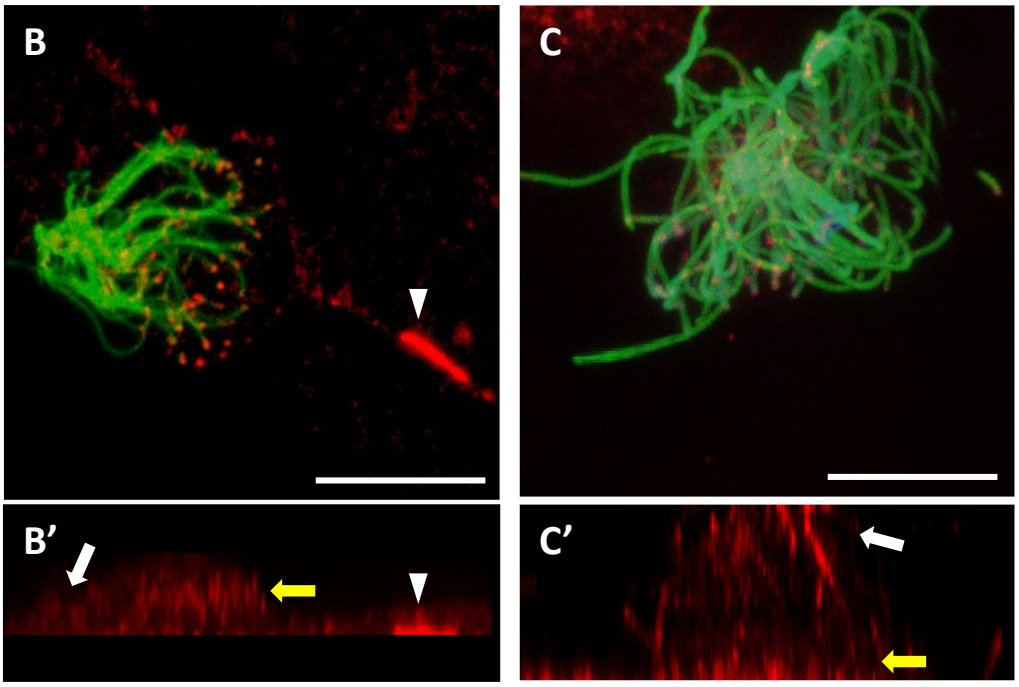

Acetylated tubulin GJA1

Figure 2

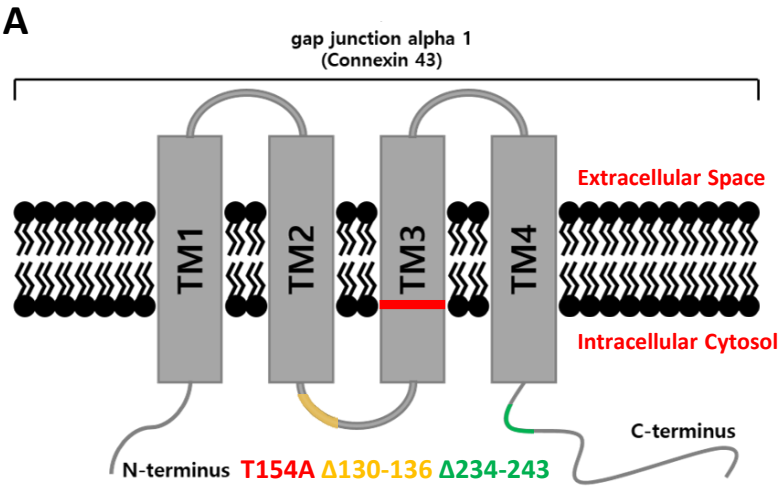
A
gap junction alpha 1
(Connexin 43)
TM1
TM2
TM3
TM4
Extracellular Space
Intracellular Cytosol
C-terminus
N-terminus T154A Δ130-136 Δ234-243

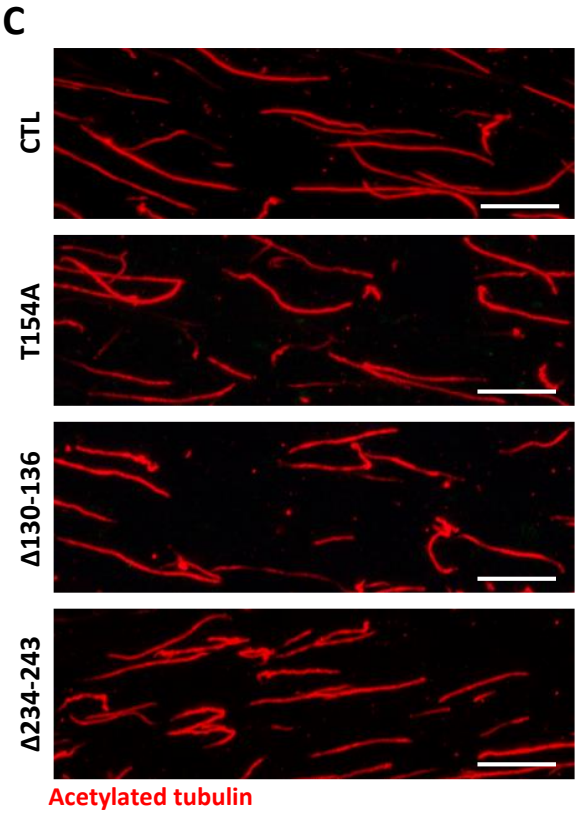
C
CTL
T154A
Δ130-136
Δ234-243
Acetylated tubulin

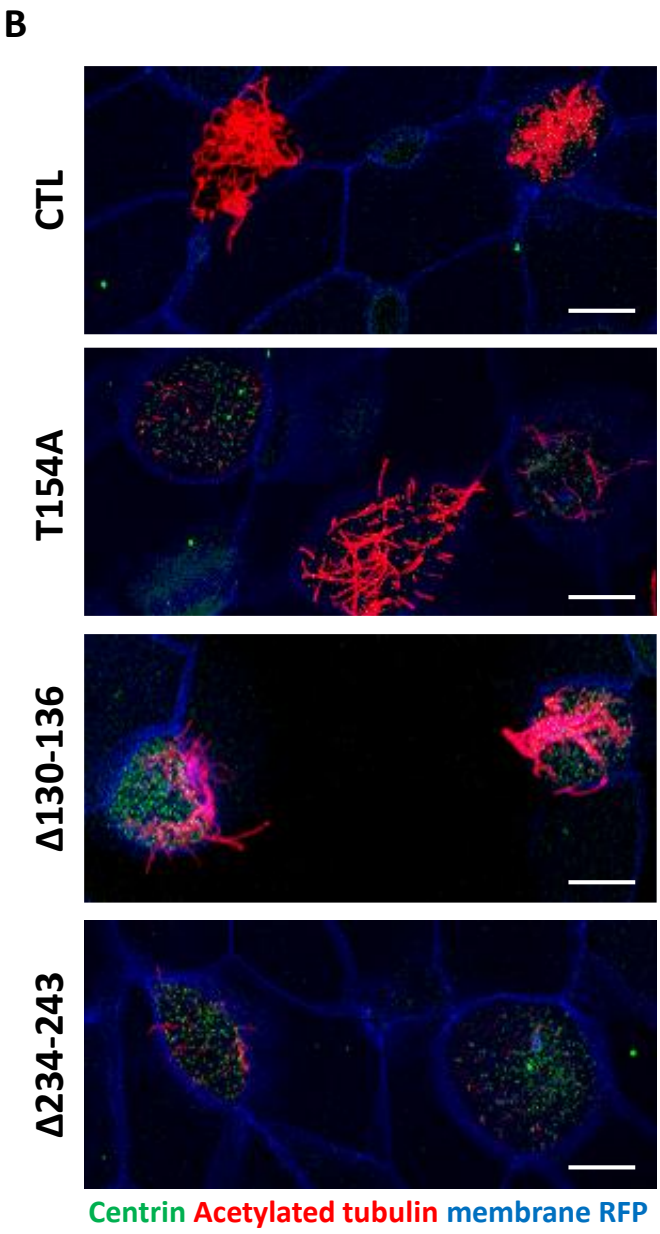
B
CTL
T154A
Δ130-136
Δ234-243
Centrin Acetylated tubulin membrane RFP

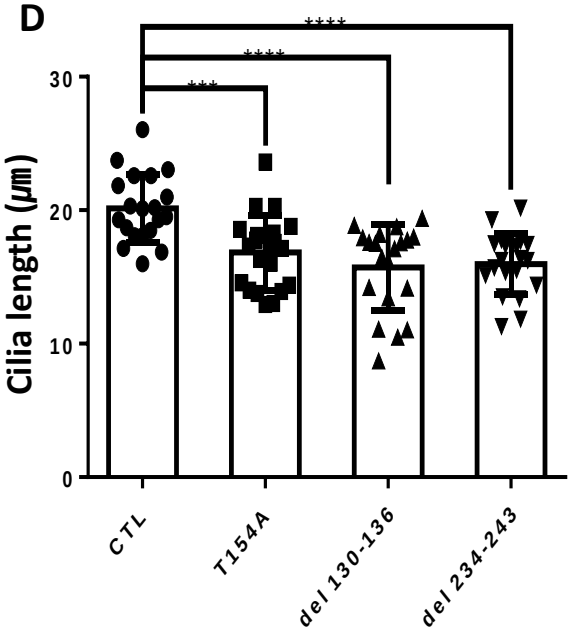
D
Cilia length (μm)
30
20
10
0
***
****
****
CTL
T154A
del 130-136
del 234-243

Figure 3

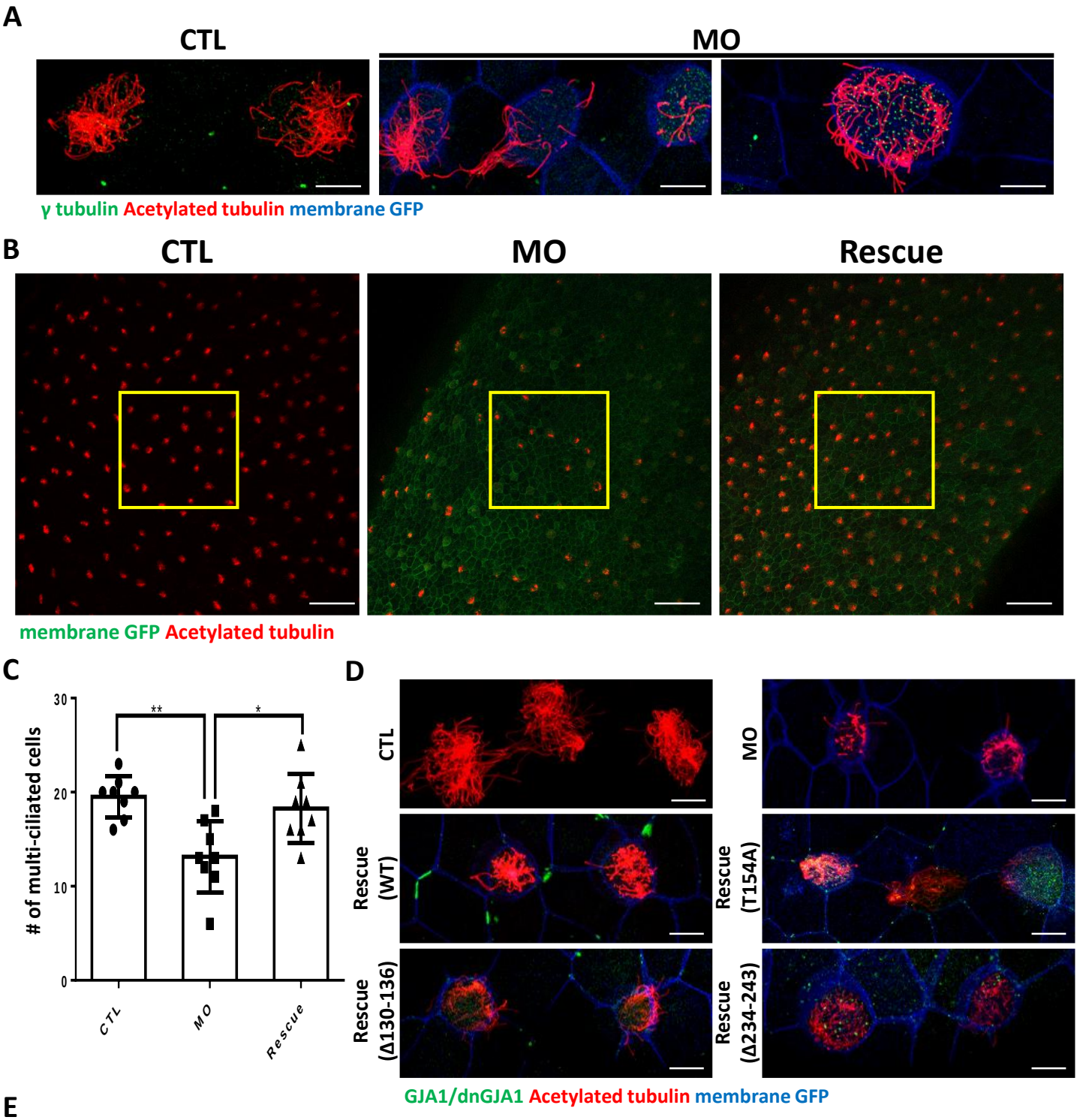
A
CTL
MO
γ tubulin Acetylated tubulin membrane GFP
B
CTL
MO
Rescue
membrane GFP Acetylated tubulin
C
# of multi-ciliated cells
30
20
10
0
**
*
CTL
MO
Rescue
D
CTL
MO
Rescue (WT)
Rescue (T154A)
Rescue (Δ130-136)
Rescue (Δ234-243)
GJA1/dnGJA1 Acetylated tubulin membrane GFP
E
MO
mRNA
wt
mis
DDDD-K
α-Tub

Figure 4

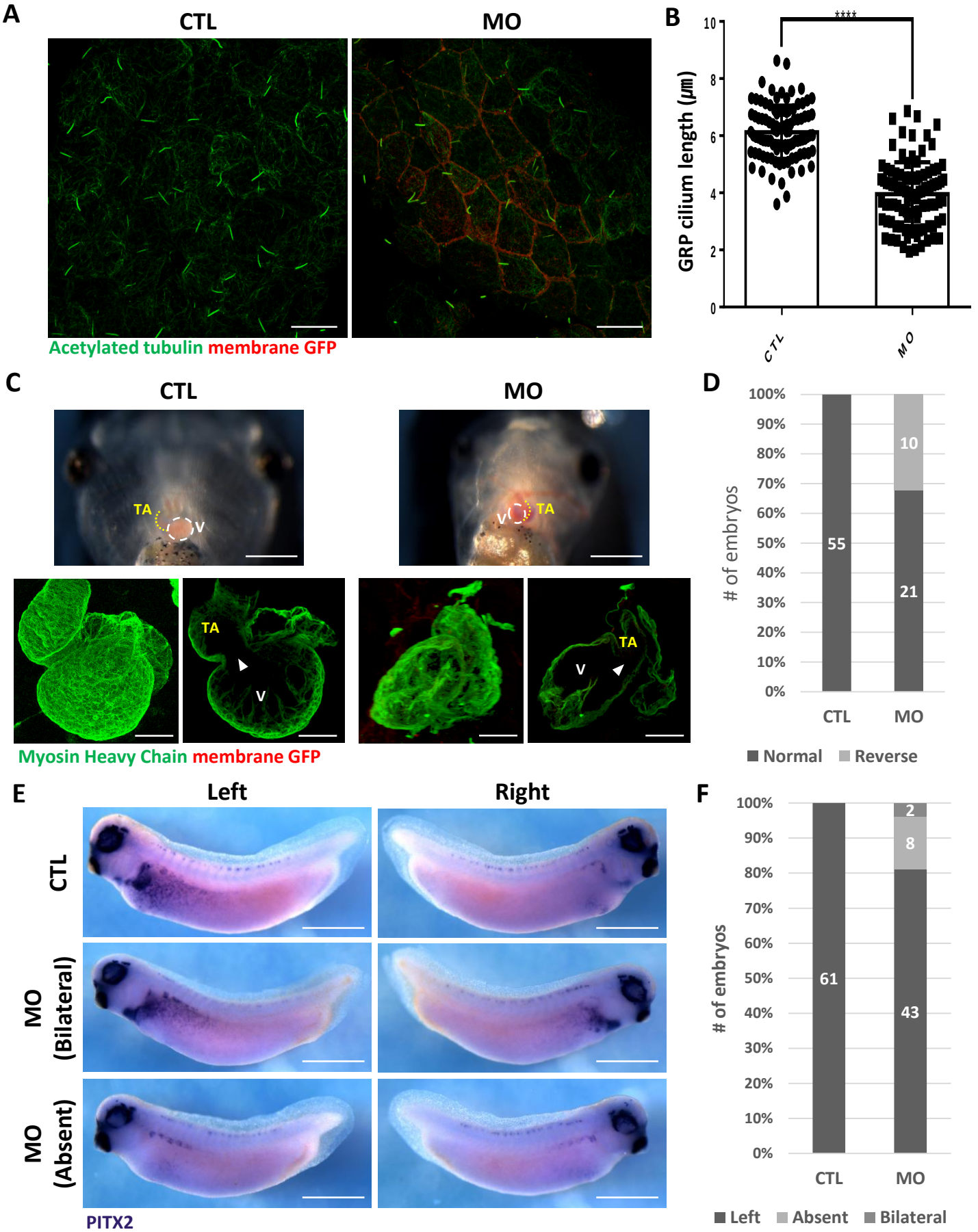
A
CTL
MO
Acetylated tubulin membrane GFP
B
****
GRP cilium length (μm)
0
2
4
6
8
10
CTL
MO
C
CTL
MO
TA
V
Myosin Heavy Chain membrane GFP
D
100%
90%
80%
70%
60%
50%
40%
30%
20%
10%
0%
# of embryos
55
10
21
CTL
MO
Normal
Reverse
E
Left
Right
CTL
MO (Bilateral)
MO (Absent)
PITX2
F
100%
90%
80%
70%
60%
50%
40%
30%
20%
10%
0%
# of embryos
61
2
8
43
CTL
MO
Left
Absent
Bilateral

Figure 5

A

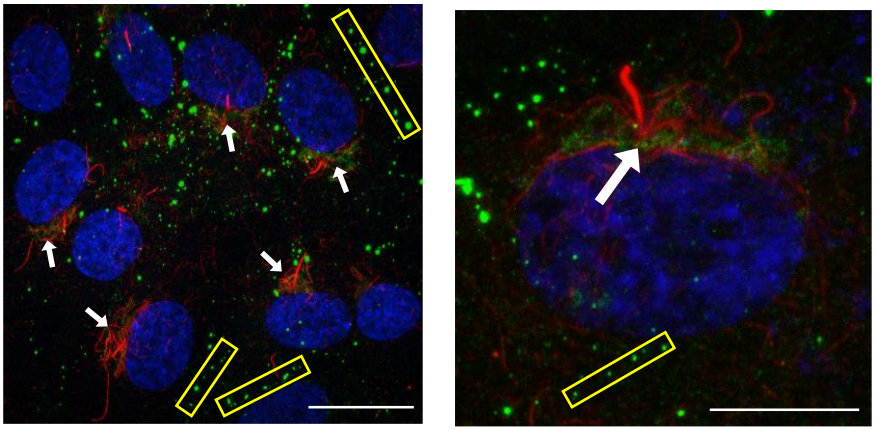

GJA1 Acetylated tubulin DAPI

B

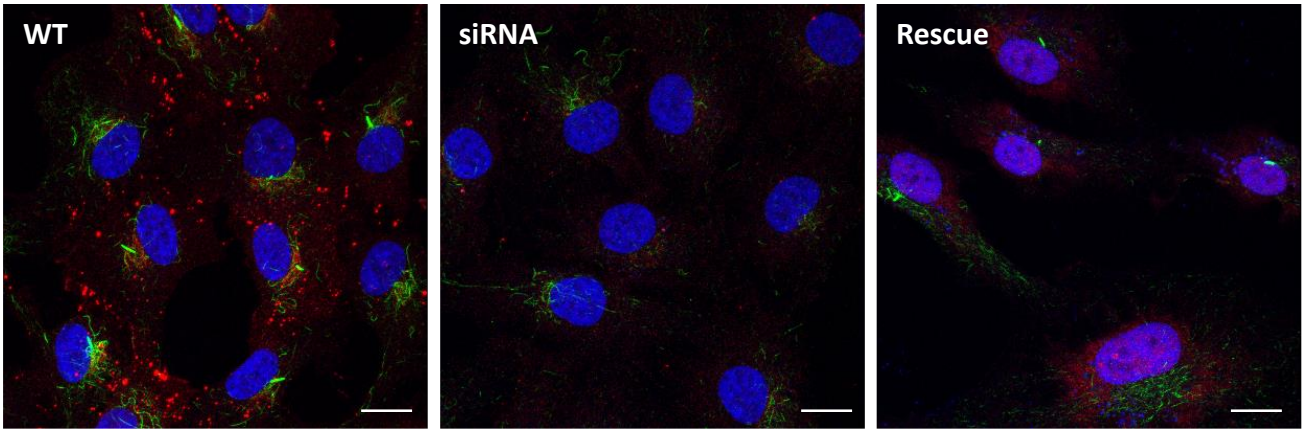

Acetylated tubulin GJA1 DAPI

C

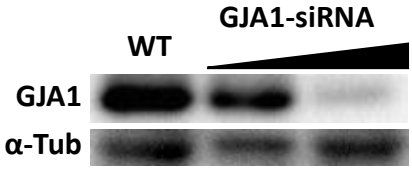

D

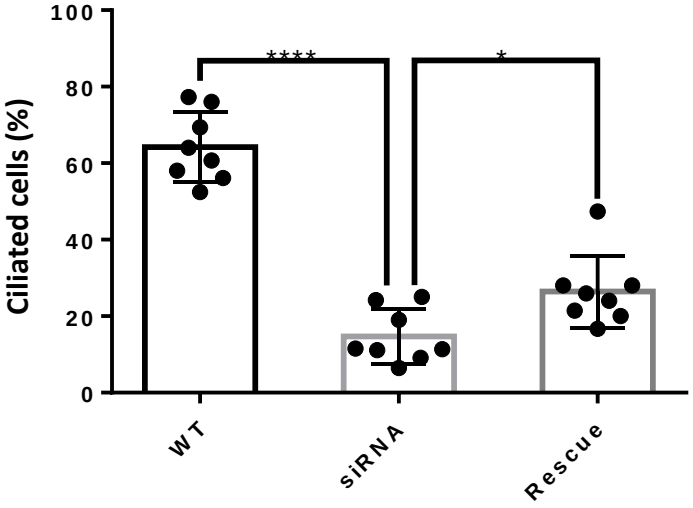

Figure 6

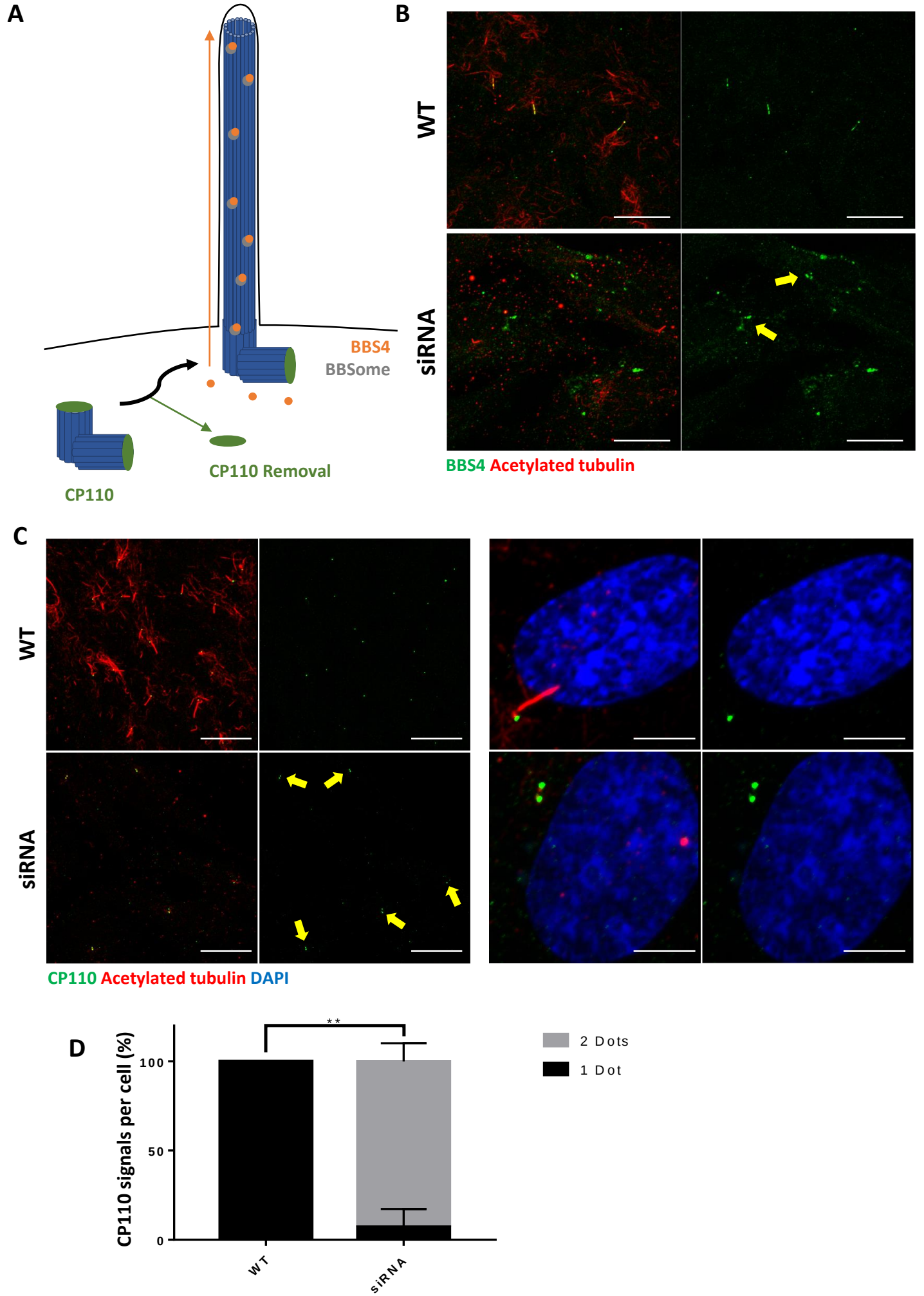
A
BBS4
BBSome
CP110 Removal
CP110
B
WT
siRNA
BBS4 Acetylated tubulin
C
WT
siRNA
CP110 Acetylated tubulin DAPI
D
CP110 signals per cell (%)
100
50
0
**
WT
siRNA
2 Dots
1 Dot

Figure 7

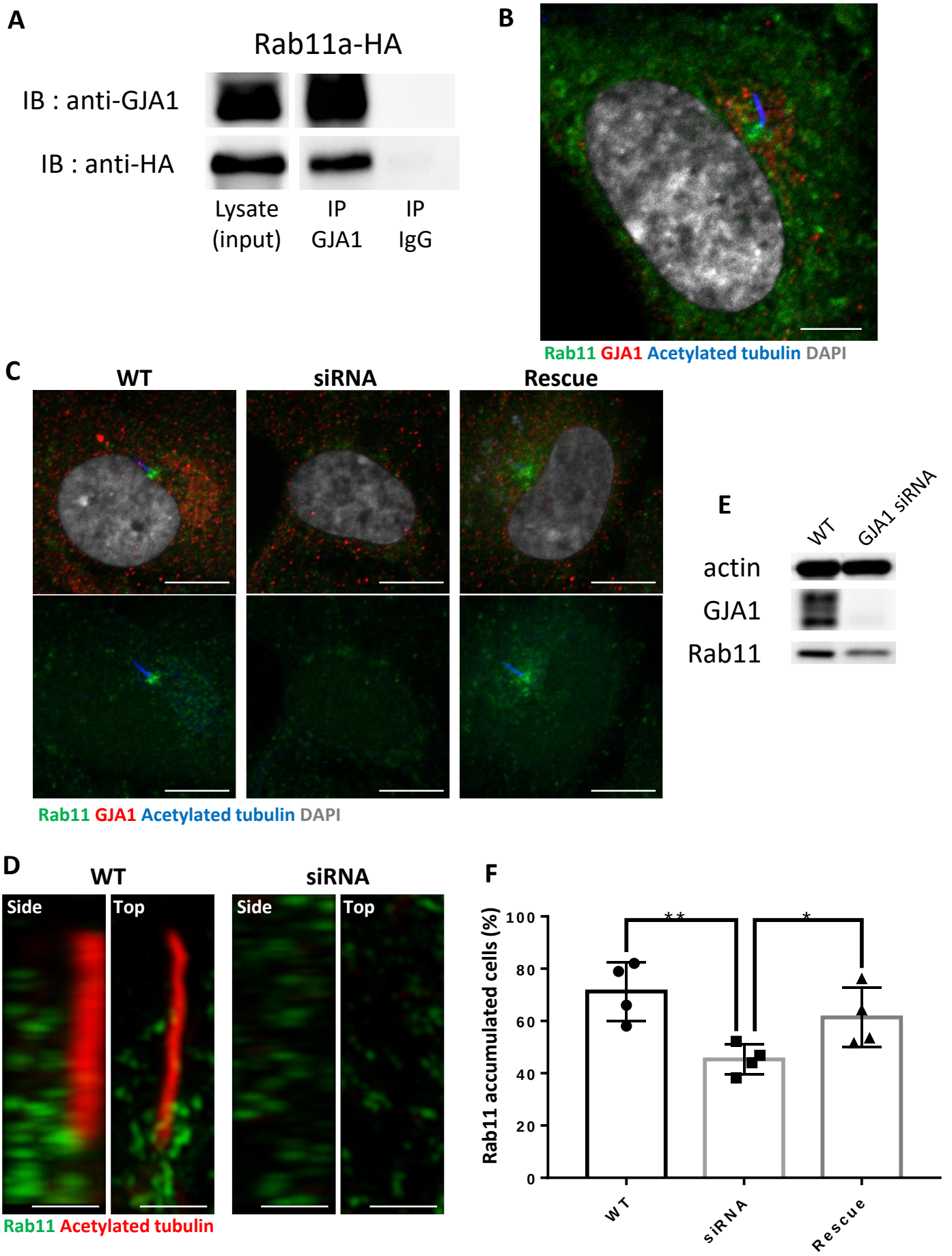
A
Rab11a-HA
IB : anti-GJA1
IB : anti-HA
Lysate (input)
IP GJA1
IP IgG
B
Rab11 GJA1 Acetylated tubulin DAPI
C
WT
siRNA
Rescue
Rab11 GJA1 Acetylated tubulin DAPI
E
WT
GJA1 siRNA
actin
GJA1
Rab11
D
WT
siRNA
Side
Top
Side
Top
Rab11 Acetylated tubulin
F
Rab11 accumulated cells (%)
100
80
60
40
20
0
**
*
WT
siRNA
Rescue

Supplementary Figures and Table

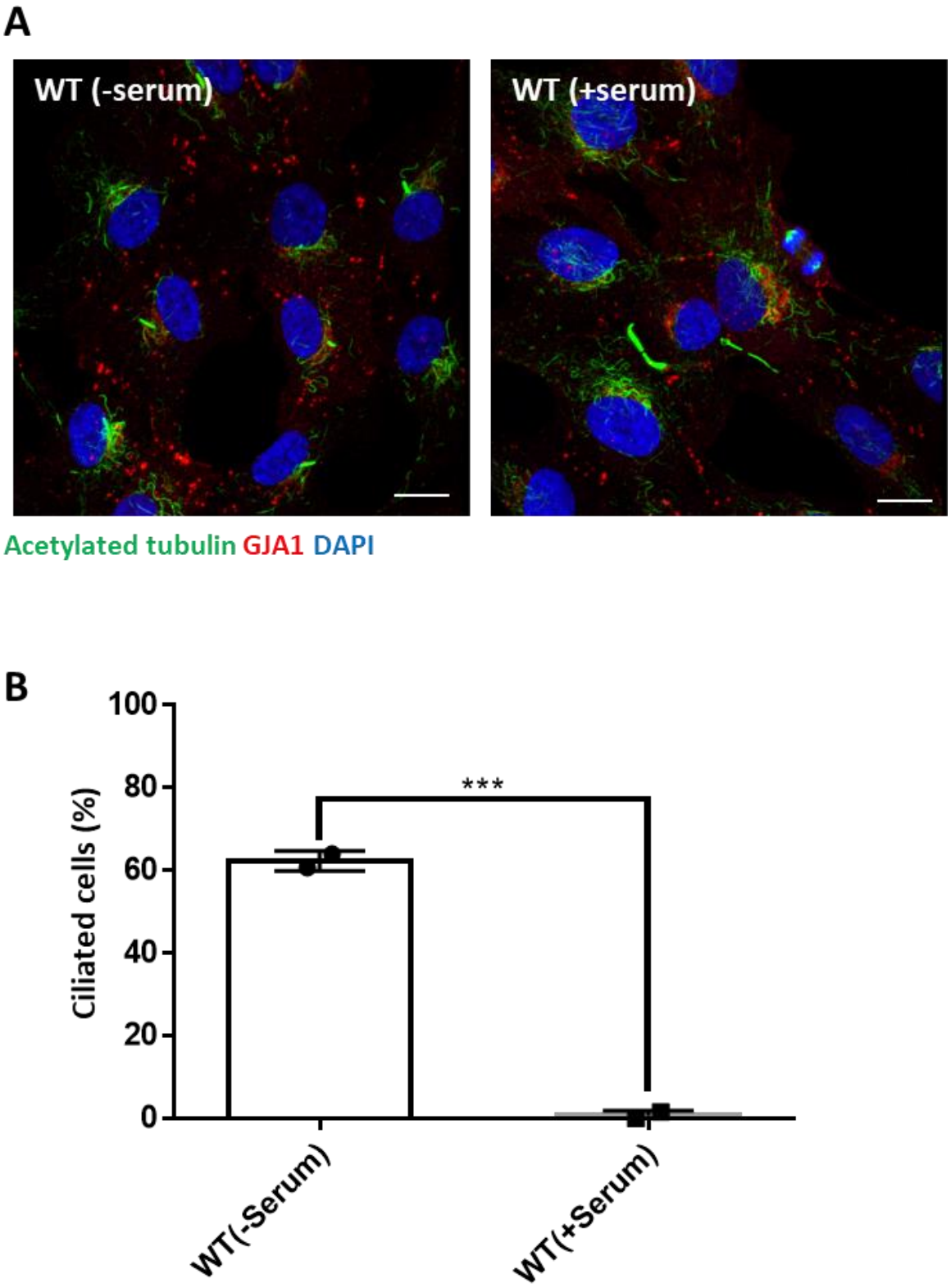

Figure S1. Ciliation of RPE1 cells by serum starvation

A. Ciliogenesis of RPE1 was induced by serum starvation. Scale bars: 10-µm.

B. Percentage of ciliated cells in (**A**) was plotted. Error bars represent mean ± s.d. (n=2 with 2 independent experiments, 1 value per experiment, Total counted cell #: -Serum=153, +Serum=125). P values were determined with the two-tailed t-test (P: ***=0.0009).

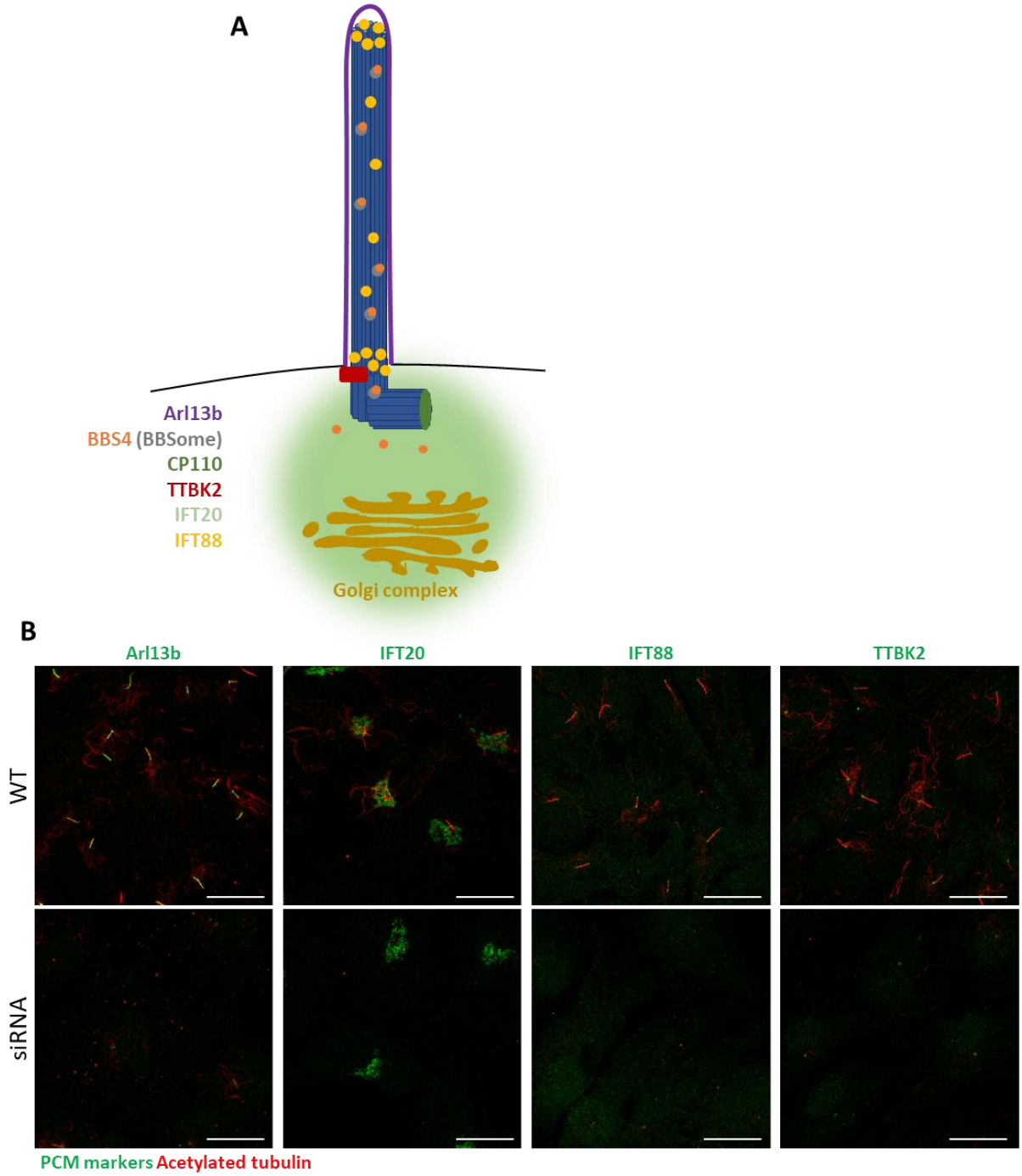

Figure S2. Cellular localization of pericentriolar material (PCM) and cilia proteins in GJA1 depleted RPE1 cells

A. Cellular localization of pericentriolar material (PCM) and ciliary proteins (Arl13B, IFT20, IFT88, and TTBK2) during ciliogenesis.

B. RPE1 cells were transfected with GJA1 siRNA and immunostained with acetylated tubulin antibody (Red) and anti-Arl13B, anti-IFT20, anti-IFT88, or anti-TTBK2 (Green) antibodies. Scale bars: 20-µm.

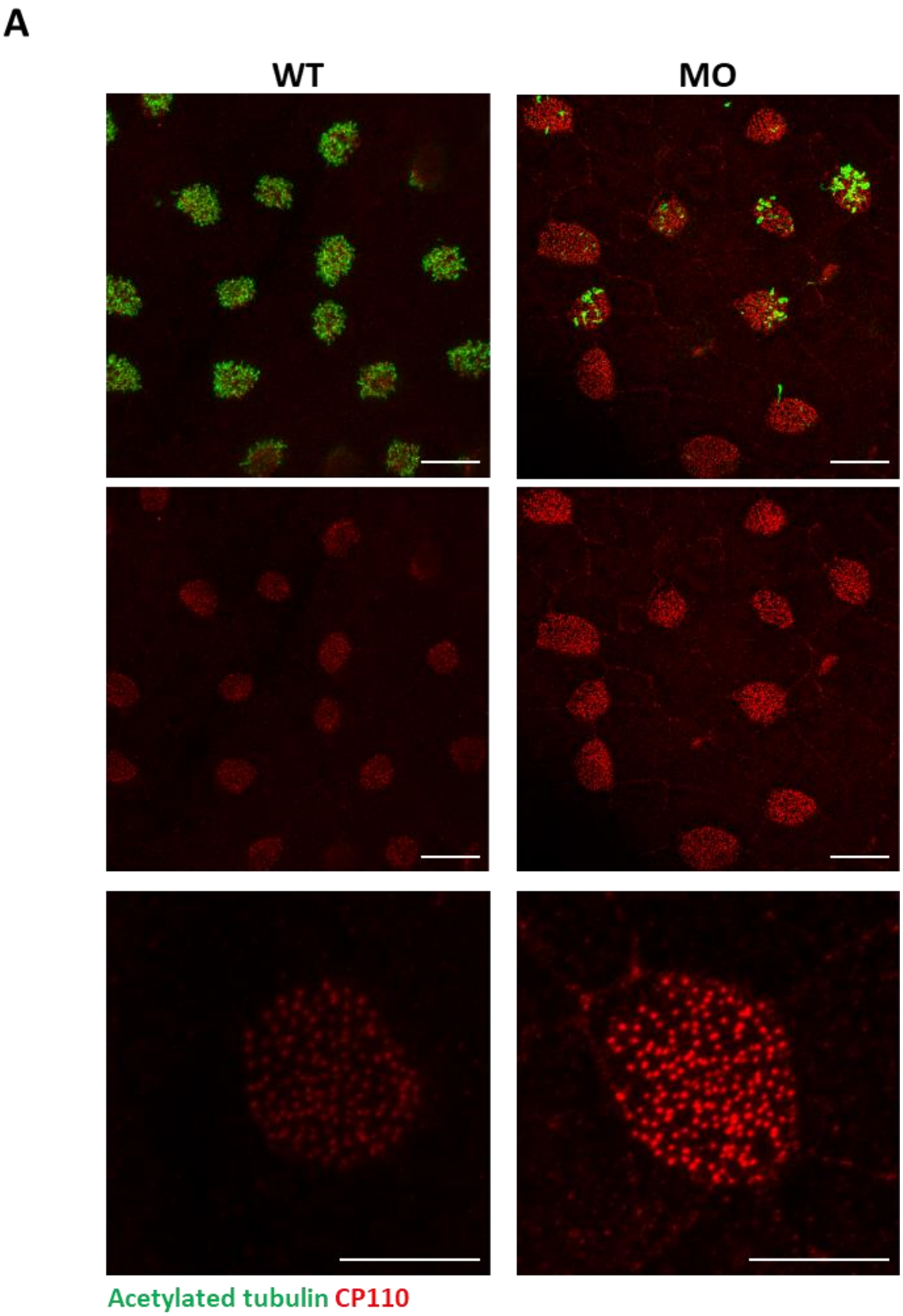

Figure S3. CP110 localization in multi-ciliated cells in GJA1-MO-injected *Xenopus* embryos

A. Wild-type (WT) and GJA1-MO-injected embryos were stained with CP110 (Red) and acetylated tubulin (Green) antibodies at stage 30. Scale bars: 20-µm (Upper, Middle panel), 10-µm (Lower panel).

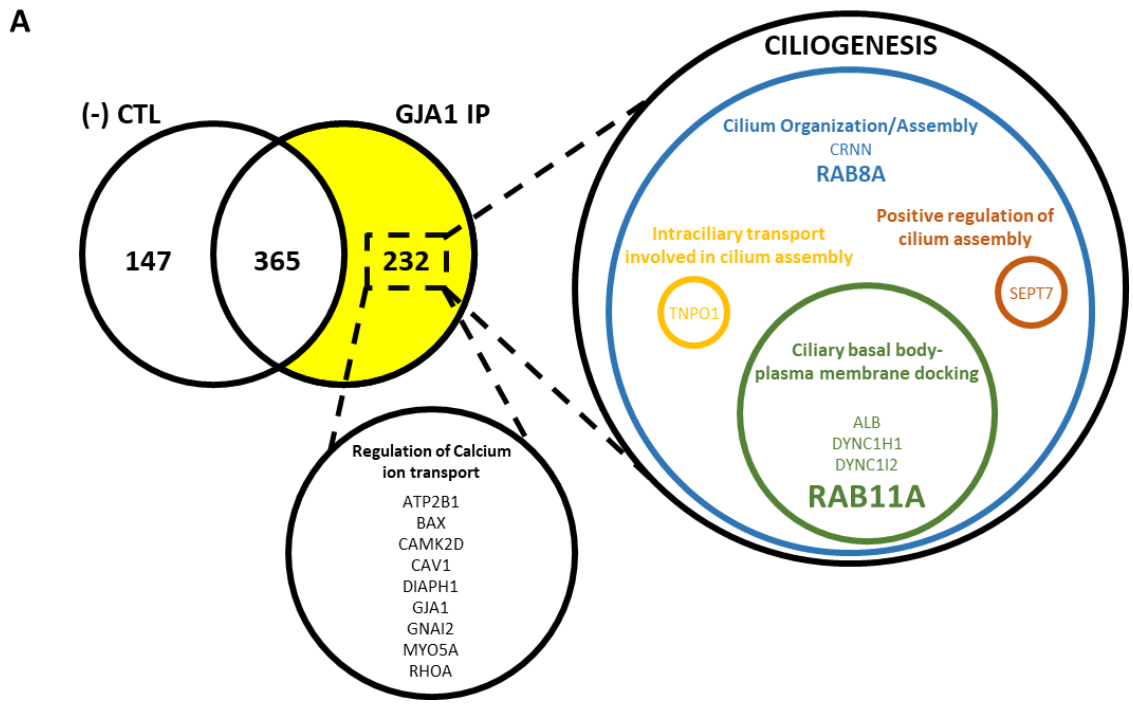

Figure S4. Identification of GJA1 interacting proteins by performing IP-MS.

A. A total of 232 proteins were detected by immunoprecipitation (IP) of GJA1 and mass spectrometry analysis. GO term analysis of the proteins identified two distinct groups of proteins involved in calcium transport and ciliogenesis.

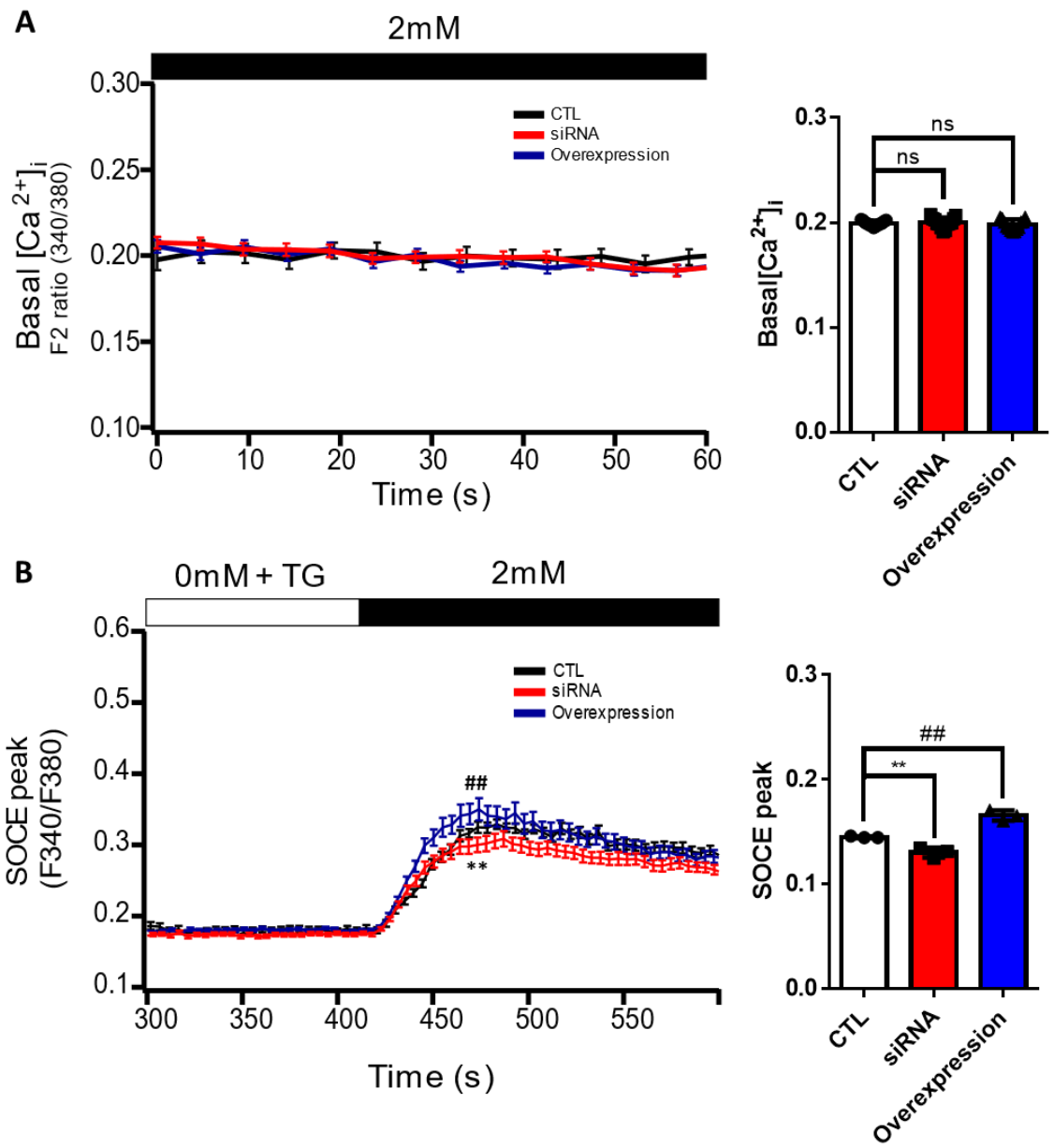

Figure S5. Basal Ca^{2+} levels and Ca^{2+} influx in GJA1 depleted RPE1 cells.

A. Basal Ca^{2+} levels in RPE1 control (CTL), hGJA1 siRNA-treated, and hGJA1-overexpressed cells were monitored by Fura-2 fluorescence ratios. Error bars represent mean ± s.d. (n=1 independent experiment, Total counted cell #: CTL=9, siRNA=33, Overexpression=34). P values were determined with one-way ANOVA (P: ns>0.05).

B. Ca^{2+} influx in RPE1 CTL, hGJA1 siRNA-treated, and hGJA1-overexpressed cells was monitored by Fura-2 fluorescence ratios. Error bars represent mean ± s.d. (n=1 independent experiment, Total counted cell #: CTL=9,

siRNA=33, Overexpression=34). P values were determined with one-way ANOVA (P: **=0.0076, ##=0.0014).

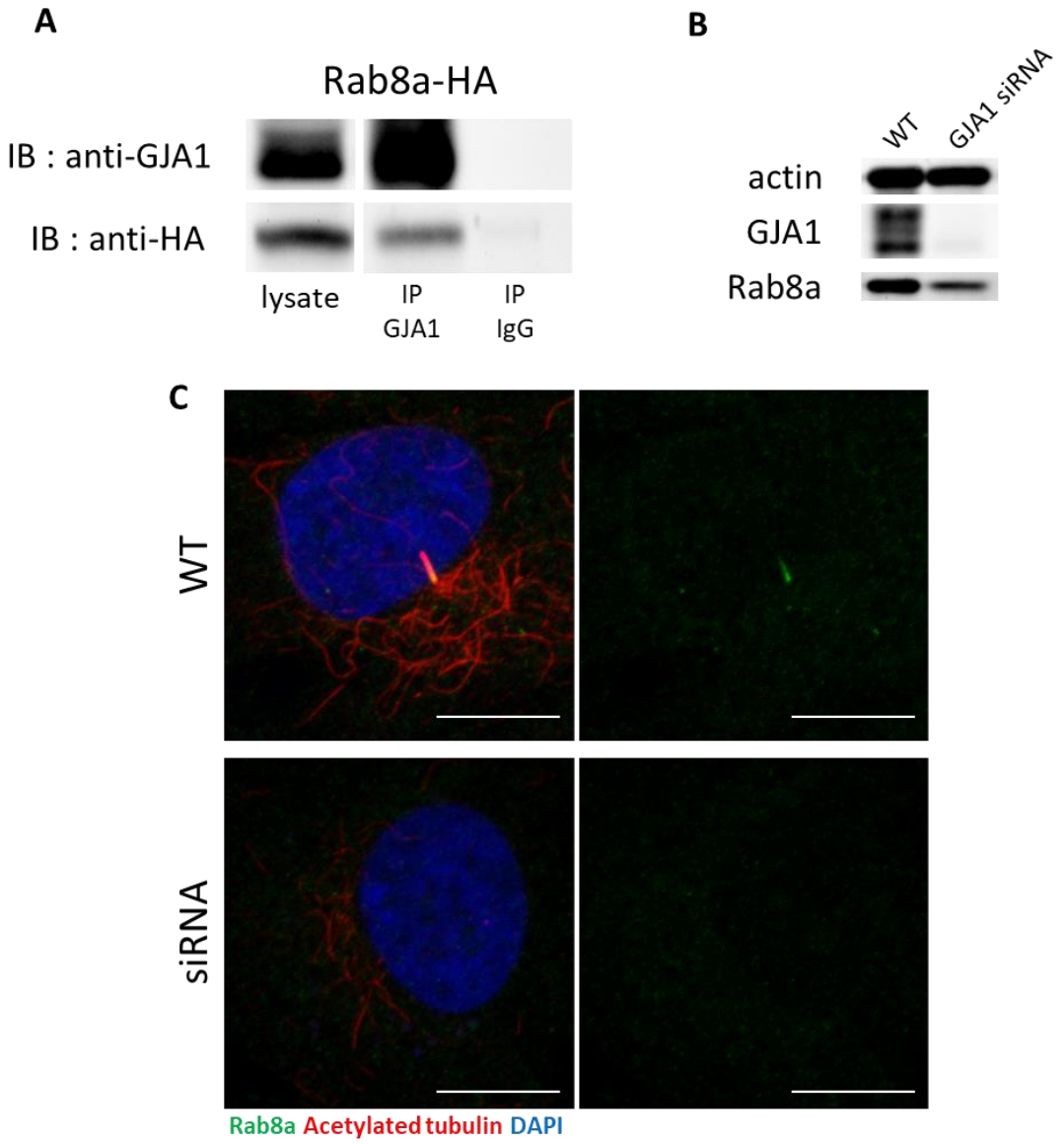

Figure S6. GJA1 interacted with Rab8a.

A. HA-tagged Rab8a protein was co-immunoprecipitated with GJA1. Immunoblotting (IB) was performed with anti-GJA1 and anti-HA antibodies.

B. Rab8a and GJA1 expression levels in GJA1 siRNA-transfected RPE1 cells. Immunoblotting was performed with GJA1 and Rab8a antibodies. Actin was used as the loading control.

C. siRNA-mediated knockdown of GJA1 inhibited Rab8a localization in RPE1 cells. RPE1 cells were labeled with anti-Rab8a antibody (Green), anti-acetylated tubulin antibody (Red), and DAPI (Blue). Scale bars: 10-μm.

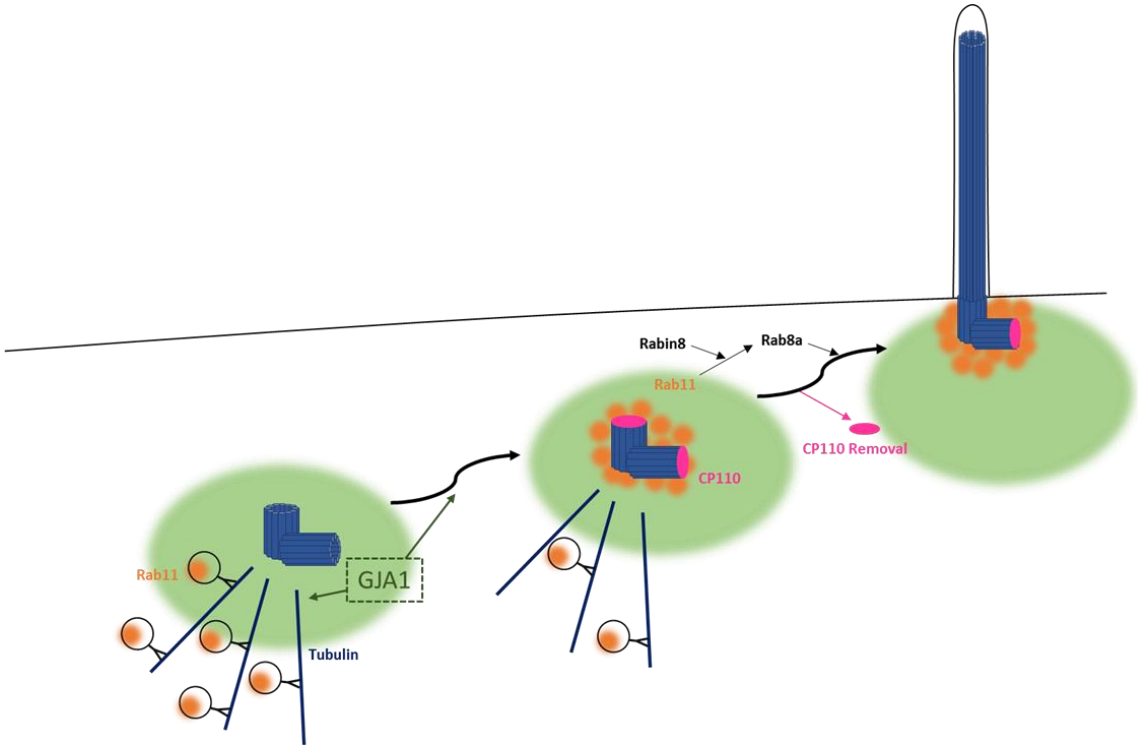

Figure S7. Suggested role of GJA1 during ciliogenesis.

GJA1 is necessary for Rab11 trafficking to the vicinity of the basal body, thereby affecting the Rabin8-Rab8a-CP110 removal cascade for ciliogenesis.

Table S1. GJA1 IP-MS results Ciliogenesis genes (**Bold**) and Ca^{2+} transport genes (*Italic*) were indicated.

Alternate ID	**Identified information**
TUBB2A	Tubulin beta-2A chain OS=Homo sapiens GN=TUBB2A PE=1 SV=1
GJA1	*Gap junction alpha-1 protein OS=Homo sapiens GN=GJA1 PE=1 SV=2*
TRIM21	E3 ubiquitin-protein ligase TRIM21 OS=Homo sapiens GN=TRIM21 PE=1 SV=1
SPTAN1	Isoform 2 of Spectrin alpha chain, non-erythrocytic 1 OS=Homo sapiens GN=SPTAN1
MYOF	Myoferlin OS=Homo sapiens GN=MYOF PE=1 SV=1
MPRIP	Isoform 2 of Myosin phosphatase Rho-interacting protein OS=Homo sapiens GN=MPRIP
IGF2R	Cation-independent mannose-6-phosphate receptor OS=Homo sapiens GN=IGF2R PE=1 SV=3
MYH13	Myosin-13 OS=Homo sapiens GN=MYH13 PE=2 SV=2
ELP4	Isoform 3 of Elongator complex protein 4 OS=Homo sapiens GN=ELP4
RPN1	Dolichyl-diphosphooligosaccharide--protein glycosyltransferase subunit 1 OS=Homo sapiens GN=RPN1 PE=1 SV=1
ALCAM	CD166 antigen OS=Homo sapiens GN=ALCAM PE=1 SV=2
ALB	**Isoform 2 of Serum albumin OS=Homo sapiens GN=ALB**
CK	(X98614) cytokeratin [Homo sapiens]
ALB	**Isoform 3 of Serum albumin OS=Homo sapiens GN=ALB**
ATP1A1	Sodium/potassium-transporting ATPase subunit alpha-1 OS=Homo sapiens GN=ATP1A1 PE=1 SV=1
ITGA3	Integrin alpha-3 OS=Homo sapiens GN=ITGA3 PE=1 SV=5
ITGAV	Integrin alpha-V OS=Homo sapiens GN=ITGAV PE=1 SV=2
NPM1	Isoform 2 of Nucleophosmin OS=Homo sapiens GN=NPM1
KRT15	Isoform 2 of Keratin, type I cytoskeletal 15 OS=Homo sapiens GN=KRT15
ITGB5	Integrin beta-5 OS=Homo sapiens GN=ITGB5 PE=1 SV=1
RAB1B	Ras-related protein Rab-1B OS=Homo sapiens GN=RAB1B PE=1 SV=1
SURF4	Surfeit locus protein 4 OS=Homo sapiens GN=SURF4 PE=1 SV=3
PPP1R18	Phostensin OS=Homo sapiens GN=PPP1R18 PE=1 SV=1

RPN2	Dolichyl-diphosphooligosaccharide--protein glycosyltransferase subunit 2 OS=Homo sapiens GN=RPN2 PE=1 SV=3
ELP5	Elongator complex protein 5 OS=Homo sapiens GN=ELP5 PE=1 SV=2
ELP6	Elongator complex protein 6 OS=Homo sapiens GN=ELP6 PE=1 SV=1
ARL6IP5	PRA1 family protein 3 OS=Homo sapiens GN=ARL6IP5 PE=1 SV=1
DYNC1I2	**Isoform 2B of Cytoplasmic dynein 1 intermediate chain 2 OS=Homo sapiens GN=DYNC1I2**
TMED9	Transmembrane emp24 domain-containing protein 9 OS=Homo sapiens GN=TMED9 PE=1 SV=2
SCFD1	Sec1 family domain-containing protein 1 OS=Homo sapiens GN=SCFD1 PE=1 SV=4
ATL3	Atlastin-3 OS=Homo sapiens GN=ATL3 PE=1 SV=1
XPO1	Exportin-1 OS=Homo sapiens GN=XPO1 PE=1 SV=1
TFRC	Transferrin receptor protein 1 OS=Homo sapiens GN=TFRC PE=1 SV=2
TXLNA	Alpha-taxilin OS=Homo sapiens GN=TXLNA PE=1 SV=3
RAB7A	Ras-related protein Rab-7a OS=Homo sapiens GN=RAB7A PE=1 SV=1
DDOST	Dolichyl-diphosphooligosaccharide--protein glycosyltransferase 48 kDa subunit OS=Homo sapiens GN=DDOST PE=1 SV=4
CAMK2D	*Isoform Delta 3 of Calcium/calmodulin-dependent protein kinase type II subunit delta OS=Homo sapiens GN=CAMK2D*
RHOA	*Transforming protein RhoA OS=Homo sapiens GN=RHOA PE=1 SV=1*
CD44	CD44 antigen OS=Homo sapiens GN=CD44 PE=1 SV=3
LGALS3BP	Galectin-3-binding protein OS=Homo sapiens GN=LGALS3BP PE=1 SV=1
MRC2	C-type mannose receptor 2 OS=Homo sapiens GN=MRC2 PE=1 SV=2
CNN2	Calponin-2 OS=Homo sapiens GN=CNN2 PE=1 SV=4
RAB8A	**Ras-related protein Rab-8A OS=Homo sapiens GN=RAB8A PE=1 SV=1**
RTN3	Reticulon-3 OS=Homo sapiens GN=RTN3 PE=1 SV=2
TNPO1	**Isoform 3 of Transportin-1 OS=Homo sapiens GN=TNPO1**
GCN1	eIF-2-alpha kinase activator GCN1 OS=Homo sapiens GN=GCN1 PE=1 SV=6
GNS	N-acetylglucosamine-6-sulfatase OS=Homo sapiens GN=GNS PE=1 SV=3

SDHA	Succinate dehydrogenase [ubiquinone] flavoprotein subunit, mitochondrial OS=Homo sapiens GN=SDHA PE=1 SV=2
ATP2B1	*Plasma membrane calcium-transporting ATPase 1 OS=Homo sapiens GN=ATP2B1 PE=1 SV=3*
TMED4	Transmembrane emp24 domain-containing protein 4 OS=Homo sapiens GN=TMED4 PE=1 SV=1
SFPQ	Splicing factor, proline- and glutamine-rich OS=Homo sapiens GN=SFPQ PE=1 SV=2
LMAN2	Vesicular integral-membrane protein VIP36 OS=Homo sapiens GN=LMAN2 PE=1 SV=1
LRRFIP2	Isoform 4 of Leucine-rich repeat flightless-interacting protein 2 OS=Homo sapiens GN=LRRFIP2
PPT1	Palmitoyl-protein thioesterase 1 OS=Homo sapiens GN=PPT1 PE=1 SV=1
FUBP1	Far upstream element-binding protein 1 OS=Homo sapiens GN=FUBP1 PE=1 SV=3
RAB11A	**Ras-related protein Rab-11A OS=Homo sapiens GN=RAB11A PE=1 SV=3**
GLG1	Golgi apparatus protein 1 OS=Homo sapiens GN=GLG1 PE=1 SV=2
ESYT1	Isoform 2 of Extended synaptotagmin-1 OS=Homo sapiens GN=ESYT1
LMNB1	Lamin-B1 OS=Homo sapiens GN=LMNB1 PE=1 SV=2
TMED10	Transmembrane emp24 domain-containing protein 10 OS=Homo sapiens GN=TMED10 PE=1 SV=2
BAX	*Isoform Sigma of Apoptosis regulator BAX OS=Homo sapiens GN=BAX*
SCCPDH	Saccharopine dehydrogenase-like oxidoreductase OS=Homo sapiens GN=SCCPDH PE=1 SV=1
CD81	CD81 antigen OS=Homo sapiens GN=CD81 PE=1 SV=1
ITGA5	Integrin alpha-5 OS=Homo sapiens GN=ITGA5 PE=1 SV=2
RAB5A	Ras-related protein Rab-5A OS=Homo sapiens GN=RAB5A PE=1 SV=2
IGLL5	Immunoglobulin lambda-like polypeptide 5 OS=Homo sapiens GN=IGLL5 PE=2 SV=2
COL27A1	Collagen alpha-1(XXVII) chain OS=Homo sapiens GN=COL27A1 PE=1 SV=1
PLBD2	Putative phospholipase B-like 2 OS=Homo sapiens GN=PLBD2 PE=1 SV=2
EPHA2	Ephrin type-A receptor 2 OS=Homo sapiens GN=EPHA2 PE=1 SV=2
MAP1B	Microtubule-associated protein 1B OS=Homo sapiens GN=MAP1B PE=1 SV=2

UQCRC2	Cytochrome b-c1 complex subunit 2, mitochondrial OS=Homo sapiens GN=UQCRC2 PE=1 SV=3
SRP68	Signal recognition particle subunit SRP68 OS=Homo sapiens GN=SRP68 PE=1 SV=2
GSR	Isoform 4 of Glutathione reductase, mitochondrial OS=Homo sapiens GN=GSR
TGOLN2	Isoform 5 of Trans-Golgi network integral membrane protein 2 OS=Homo sapiens GN=TGOLN2
GIPC1	PDZ domain-containing protein GIPC1 OS=Homo sapiens GN=GIPC1 PE=1 SV=2
SERPINB3	Serpin B3 OS=Homo sapiens GN=SERPINB3 PE=1 SV=2
DBNL	Isoform 2 of Drebrin-like protein OS=Homo sapiens GN=DBNL
PCYOX1	Isoform 2 of Prenylcysteine oxidase 1 OS=Homo sapiens GN=PCYOX1
TICAM2	Isoform 2 of TIR domain-containing adapter molecule 2 OS=Homo sapiens GN=TICAM2
PIGR	Polymeric immunoglobulin receptor OS=Homo sapiens GN=PIGR PE=1 SV=4
ATP5F1	ATP synthase F(0) complex subunit B1, mitochondrial OS=Homo sapiens GN=ATP5F1 PE=1 SV=2
HACD3	Very-long-chain (3R)-3-hydroxyacyl-CoA dehydratase 3 OS=Homo sapiens GN=HACD3 PE=1 SV=2
SCARB2	Isoform 2 of Lysosome membrane protein 2 OS=Homo sapiens GN=SCARB2
PSMA4	Proteasome subunit alpha type-4 OS=Homo sapiens GN=PSMA4 PE=1 SV=1
SLC25A3	Isoform B of Phosphate carrier protein, mitochondrial OS=Homo sapiens GN=SLC25A3
HLA-A	HLA class I histocompatibility antigen, A-2 alpha chain OS=Homo sapiens GN=HLA-A PE=1 SV=1
SERPINB12	Serpin B12 OS=Homo sapiens GN=SERPINB12 PE=1 SV=1
TMEM106B	Transmembrane protein 106B OS=Homo sapiens GN=TMEM106B PE=1 SV=2
RAB2A	Ras-related protein Rab-2A OS=Homo sapiens GN=RAB2A PE=1 SV=1
AHCY	Adenosylhomocysteinase OS=Homo sapiens GN=AHCY PE=1 SV=4
PDLIM2	Isoform 5 of PDZ and LIM domain protein 2 OS=Homo sapiens GN=PDLIM2
S100A8	Protein S100-A8 OS=Homo sapiens GN=S100A8 PE=1 SV=1
EIF3F	Eukaryotic translation initiation factor 3 subunit F OS=Homo sapiens GN=EIF3F PE=1 SV=1
TBC1D15	Isoform 3 of TBC1 domain family member 15 OS=Homo sapiens GN=TBC1D15

CAV1	*Caveolin-1 OS=Homo sapiens GN=CAV1 PE=1 SV=4*
SCAMP1	Secretory carrier-associated membrane protein 1 OS=Homo sapiens GN=SCAMP1 PE=1 SV=2
HYOU1	Hypoxia up-regulated protein 1 OS=Homo sapiens GN=HYOU1 PE=1 SV=1
HTRA1	Serine protease HTRA1 OS=Homo sapiens GN=HTRA1 PE=1 SV=1
RPS12	40S ribosomal protein S12 OS=Homo sapiens GN=RPS12 PE=1 SV=3
PSMC5	26S protease regulatory subunit 8 OS=Homo sapiens GN=PSMC5 PE=1 SV=1
TPD52L2	Tumor protein D54 OS=Homo sapiens GN=TPD52L2 PE=1 SV=2
RDH11	Retinol dehydrogenase 11 OS=Homo sapiens GN=RDH11 PE=1 SV=2
TM9SF3	Transmembrane 9 superfamily member 3 OS=Homo sapiens GN=TM9SF3 PE=1 SV=2
PDLIM4	PDZ and LIM domain protein 4 OS=Homo sapiens GN=PDLIM4 PE=1 SV=2
GOLT1B	Vesicle transport protein GOT1B OS=Homo sapiens GN=GOLT1B PE=1 SV=1
CSN3	KAPPA CASEIN PRECURSOR. - BOS TAURUS (BOVINE).
RER1	Protein RER1 OS=Homo sapiens GN=RER1 PE=1 SV=1
ATP6V1E1	Isoform 2 of V-type proton ATPase subunit E 1 OS=Homo sapiens GN=ATP6V1E1
ADAM9	Disintegrin and metalloproteinase domain-containing protein 9 OS=Homo sapiens GN=ADAM9 PE=1 SV=1
STMN1	Stathmin OS=Homo sapiens GN=STMN1 PE=1 SV=3
CD63	Isoform 3 of CD63 antigen OS=Homo sapiens GN=CD63
MYO5A	*Unconventional myosin-Va OS=Homo sapiens GN=MYO5A PE=1 SV=2*
RPL31	60S ribosomal protein L31 OS=Homo sapiens GN=RPL31 PE=1 SV=1
B2M	Beta-2-microglobulin OS=Homo sapiens GN=B2M PE=1 SV=1
DYNC1H1	**Cytoplasmic dynein 1 heavy chain 1 OS=Homo sapiens GN=DYNC1H1 PE=1 SV=5**
ERAP1	Endoplasmic reticulum aminopeptidase 1 OS=Homo sapiens GN=ERAP1 PE=1 SV=3
GBF1	Golgi-specific brefeldin A-resistance guanine nucleotide exchange factor 1 OS=Homo sapiens GN=GBF1 PE=1 SV=2
NUP153	Nuclear pore complex protein Nup153 OS=Homo sapiens GN=NUP153 PE=1 SV=2
COL3A1	Collagen alpha-1(III) chain OS=Homo sapiens GN=COL3A1 PE=1 SV=4
PSMD4	26S proteasome non-ATPase regulatory subunit 4 OS=Homo sapiens GN=PSMD4 PE=1

	SV=1
LPCAT2	Lysophosphatidylcholine acyltransferase 2 OS=Homo sapiens GN=LPCAT2 PE=1 SV=1
PSMD11	26S proteasome non-ATPase regulatory subunit 11 OS=Homo sapiens GN=PSMD11 PE=1 SV=3
PSMC3	26S protease regulatory subunit 6A OS=Homo sapiens GN=PSMC3 PE=1 SV=3
USP5	Ubiquitin carboxyl-terminal hydrolase 5 OS=Homo sapiens GN=USP5 PE=1 SV=2
PNP	Purine nucleoside phosphorylase OS=Homo sapiens GN=PNP PE=1 SV=2
USP31	Ubiquitin carboxyl-terminal hydrolase 31 OS=Homo sapiens GN=USP31 PE=2 SV=2
ATP6V1C1	V-type proton ATPase subunit C 1 OS=Homo sapiens GN=ATP6V1C1 PE=1 SV=4
MAN2B2	Epididymis-specific alpha-mannosidase OS=Homo sapiens GN=MAN2B2 PE=1 SV=4
SLC3A2	4F2 cell-surface antigen heavy chain OS=Homo sapiens GN=SLC3A2 PE=1 SV=3
RPS10	40S ribosomal protein S10 OS=Homo sapiens GN=RPS10 PE=1 SV=1
ACSL3	Long-chain-fatty-acid--CoA ligase 3 OS=Homo sapiens GN=ACSL3 PE=1 SV=3
RETSAT	All-trans-retinol 13,14-reductase OS=Homo sapiens GN=RETSAT PE=1 SV=2
SENP5	Sentrin-specific protease 5 OS=Homo sapiens GN=SENP5 PE=1 SV=3
TRAF3	TNF receptor-associated factor 3 OS=Homo sapiens GN=TRAF3 PE=1 SV=2
ATP2A2	Sarcoplasmic/endoplasmic reticulum calcium ATPase 2 OS=Homo sapiens GN=ATP2A2 PE=1 SV=1
SEPT7	**Septin-7 OS=Homo sapiens GN=SEPT7 PE=1 SV=2**
HNRNPM	Heterogeneous nuclear ribonucleoprotein M OS=Homo sapiens GN=HNRNPM PE=1 SV=3
ALDH3A2	Isoform 2 of Fatty aldehyde dehydrogenase OS=Homo sapiens GN=ALDH3A2
DYNC1LI1	Cytoplasmic dynein 1 light intermediate chain 1 OS=Homo sapiens GN=DYNC1LI1 PE=1 SV=3
CSN1S2	ALPHA-S2 CASEIN PRECURSOR. - BOS TAURUS (BOVINE).
MYADM	Myeloid-associated differentiation marker OS=Homo sapiens GN=MYADM PE=1 SV=2
MOGS	Isoform 2 of Mannosyl-oligosaccharide glucosidase OS=Homo sapiens GN=MOGS
BCAP31	B-cell receptor-associated protein 31 OS=Homo sapiens GN=BCAP31 PE=1 SV=3
COMT	Catechol O-methyltransferase OS=Homo sapiens GN=COMT PE=1 SV=2
SEC31A	Protein transport protein Sec31A OS=Homo sapiens GN=SEC31A PE=1 SV=3

ADRM1	Proteasomal ubiquitin receptor ADRM1 OS=Homo sapiens GN=ADRM1 PE=1 SV=2
KRT9	ct|1082558-DECOY|S41161 keratin 9, cytoskeletal - human
EEA1	Early endosome antigen 1 OS=Homo sapiens GN=EEA1 PE=1 SV=2
SLC2A1	Solute carrier family 2, facilitated glucose transporter member 1 OS=Homo sapiens GN=SLC2A1 PE=1 SV=2
HSPH1	Heat shock protein 105 kDa OS=Homo sapiens GN=HSPH1 PE=1 SV=1
PIP	Prolactin-inducible protein OS=Homo sapiens GN=PIP PE=1 SV=1
MFGE8	Lactadherin OS=Homo sapiens GN=MFGE8 PE=1 SV=2
FASN	Fatty acid synthase OS=Homo sapiens GN=FASN PE=1 SV=3
ANKS1A	Ankyrin repeat and SAM domain-containing protein 1A OS=Homo sapiens GN=ANKS1A PE=1 SV=4
LMAN1	Protein ERGIC-53 OS=Homo sapiens GN=LMAN1 PE=1 SV=2
VDAC1	Voltage-dependent anion-selective channel protein 1 OS=Homo sapiens GN=VDAC1 PE=1 SV=2
MLEC	Malectin OS=Homo sapiens GN=MLEC PE=1 SV=1
SEL1L	Protein sel-1 homolog 1 OS=Homo sapiens GN=SEL1L PE=1 SV=3
ADAM10	Disintegrin and metalloproteinase domain-containing protein 10 OS=Homo sapiens GN=ADAM10 PE=1 SV=1
DIAPH1	*Isoform 3 of Protein diaphanous homolog 1 OS=Homo sapiens GN=DIAPH1*
ESYT2	Isoform 2 of Extended synaptotagmin-2 OS=Homo sapiens GN=ESYT2
NNT	NAD(P) transhydrogenase, mitochondrial OS=Homo sapiens GN=NNT PE=1 SV=3
GAS6	Growth arrest-specific protein 6 OS=Homo sapiens GN=GAS6 PE=1 SV=2
RAC1	Isoform B of Ras-related C3 botulinum toxin substrate 1 OS=Homo sapiens GN=RAC1
RPL34	60S ribosomal protein L34 OS=Homo sapiens GN=RPL34 PE=1 SV=3
CSTB	Cystatin-B OS=Homo sapiens GN=CSTB PE=1 SV=2
CTSZ	Cathepsin Z OS=Homo sapiens GN=CTSZ PE=1 SV=1
TMEM43	Transmembrane protein 43 OS=Homo sapiens GN=TMEM43 PE=1 SV=1
SH3BP4	SH3 domain-binding protein 4 OS=Homo sapiens GN=SH3BP4 PE=1 SV=1
CBR1	Carbonyl reductase [NADPH] 1 OS=Homo sapiens GN=CBR1 PE=1 SV=3

FAP	Prolyl endopeptidase FAP OS=Homo sapiens GN=FAP PE=1 SV=5
NEDD4L	E3 ubiquitin-protein ligase NEDD4-like OS=Homo sapiens GN=NEDD4L PE=1 SV=2
HIP1	Huntingtin-interacting protein 1 OS=Homo sapiens GN=HIP1 PE=1 SV=5
GPD2	Glycerol-3-phosphate dehydrogenase, mitochondrial OS=Homo sapiens GN=GPD2 PE=1 SV=3
HADHB	Trifunctional enzyme subunit beta, mitochondrial OS=Homo sapiens GN=HADHB PE=1 SV=3
PSMB6	Proteasome subunit beta type-6 OS=Homo sapiens GN=PSMB6 PE=1 SV=4
STX7	Syntaxin-7 OS=Homo sapiens GN=STX7 PE=1 SV=4
ITGA2	Integrin alpha-2 OS=Homo sapiens GN=ITGA2 PE=1 SV=1
PDLIM1	PDZ and LIM domain protein 1 OS=Homo sapiens GN=PDLIM1 PE=1 SV=4
GOLIM4	Golgi integral membrane protein 4 OS=Homo sapiens GN=GOLIM4 PE=1 SV=1
ST13	Hsc70-interacting protein OS=Homo sapiens GN=ST13 PE=1 SV=2
GPR180	Integral membrane protein GPR180 OS=Homo sapiens GN=GPR180 PE=2 SV=1
IPO7	Importin-7 OS=Homo sapiens GN=IPO7 PE=1 SV=1
FARSB	Phenylalanine--tRNA ligase beta subunit OS=Homo sapiens GN=FARSB PE=1 SV=3
IPO5	Isoform 3 of Importin-5 OS=Homo sapiens GN=IPO5
IMPAD1	Inositol monophosphatase 3 OS=Homo sapiens GN=IMPAD1 PE=1 SV=1
ETFB	Electron transfer flavoprotein subunit beta OS=Homo sapiens GN=ETFB PE=1 SV=3
BLMH	Bleomycin hydrolase OS=Homo sapiens GN=BLMH PE=1 SV=1
S100A14	Protein S100-A14 OS=Homo sapiens GN=S100A14 PE=1 SV=1
TOMM70	Mitochondrial import receptor subunit TOM70 OS=Homo sapiens GN=TOMM70 PE=1 SV=1
GLIPR1L1	sp|Q6UWM5-DECOY|GPRL1_HUMAN GLIPR1-like protein 1 OS=Homo sapiens GN=GLIPR1L1 PE=1...
DDX60	Probable ATP-dependent RNA helicase DDX60 OS=Homo sapiens GN=DDX60 PE=1 SV=3
GNAI2	*Guanine nucleotide-binding protein G(i) subunit alpha-2 OS=Homo sapiens GN=GNAI2 PE=1 SV=3*
SLC25A6	ADP/ATP translocase 3 OS=Homo sapiens GN=SLC25A6 PE=1 SV=4

FTL	Ferritin light chain OS=Homo sapiens GN=FTL PE=1 SV=2
JMY	Isoform 2 of Junction-mediating and -regulatory protein OS=Homo sapiens GN=JMY
ESD	S-formylglutathione hydrolase OS=Homo sapiens GN=ESD PE=1 SV=2
FAM3C	Protein FAM3C OS=Homo sapiens GN=FAM3C PE=1 SV=1
PSAP	Prosaposin OS=Homo sapiens GN=PSAP PE=1 SV=2
CYB5R3	NADH-cytochrome b5 reductase 3 OS=Homo sapiens GN=CYB5R3 PE=1 SV=3
EIF4A2	Eukaryotic initiation factor 4A-II OS=Homo sapiens GN=EIF4A2 PE=1 SV=2
CD276	CD276 antigen OS=Homo sapiens GN=CD276 PE=1 SV=1
CRNN	**Cornulin OS=Homo sapiens GN=CRNN PE=1 SV=1**
HLA-A	HLA class I histocompatibility antigen, A-1 alpha chain OS=Homo sapiens GN=HLA-A PE=1 SV=1
ERLIN1	Erlin-1 OS=Homo sapiens GN=ERLIN1 PE=1 SV=1
SEC11A	Signal peptidase complex catalytic subunit SEC11A OS=Homo sapiens GN=SEC11A PE=1 SV=1
ERGIC3	Endoplasmic reticulum-Golgi intermediate compartment protein 3 OS=Homo sapiens GN=ERGIC3 PE=1 SV=1
MARS	Methionine--tRNA ligase, cytoplasmic OS=Homo sapiens GN=MARS PE=1 SV=2
ACAT1	Acetyl-CoA acetyltransferase, mitochondrial OS=Homo sapiens GN=ACAT1 PE=1 SV=1
PSMD2	26S proteasome non-ATPase regulatory subunit 2 OS=Homo sapiens GN=PSMD2 PE=1 SV=3
HNRNPCL2	Heterogeneous nuclear ribonucleoprotein C-like 2 OS=Homo sapiens GN=HNRNPCL2 PE=1 SV=1
MAN2B1	Lysosomal alpha-mannosidase OS=Homo sapiens GN=MAN2B1 PE=1 SV=3
EIF3H	Eukaryotic translation initiation factor 3 subunit H OS=Homo sapiens GN=EIF3H PE=1 SV=1
DNAJB6	Isoform B of DnaJ homolog subfamily B member 6 OS=Homo sapiens GN=DNAJB6
IGKC	Ig kappa chain C region OS=Homo sapiens GN=IGKC PE=1 SV=1
LTF	Lactotransferrin OS=Homo sapiens GN=LTF PE=1 SV=6
SMPD1	Sphingomyelin phosphodiesterase OS=Homo sapiens GN=SMPD1 PE=1 SV=4

PSMB1	Proteasome subunit beta type-1 OS=Homo sapiens GN=PSMB1 PE=1 SV=2
PSMA3	Isoform 2 of Proteasome subunit alpha type-3 OS=Homo sapiens GN=PSMA3
CALML3	Calmodulin-like protein 3 OS=Homo sapiens GN=CALML3 PE=1 SV=2
MAT2A	S-adenosylmethionine synthase isoform type-2 OS=Homo sapiens GN=MAT2A PE=1 SV=1
RPS5	40S ribosomal protein S5 OS=Homo sapiens GN=RPS5 PE=1 SV=4
TMEM33	Transmembrane protein 33 OS=Homo sapiens GN=TMEM33 PE=1 SV=2
LBR	Lamin-B receptor OS=Homo sapiens GN=LBR PE=1 SV=2
SPCS2	Signal peptidase complex subunit 2 OS=Homo sapiens GN=SPCS2 PE=1 SV=3
SF3B4	Splicing factor 3B subunit 4 OS=Homo sapiens GN=SF3B4 PE=1 SV=1
SLC30A7	Zinc transporter 7 OS=Homo sapiens GN=SLC30A7 PE=2 SV=1
SRPK1	SRSF protein kinase 1 OS=Homo sapiens GN=SRPK1 PE=1 SV=2
SDF2	Stromal cell-derived factor 2 OS=Homo sapiens GN=SDF2 PE=1 SV=2
VKORC1	Vitamin K epoxide reductase complex subunit 1 OS=Homo sapiens GN=VKORC1 PE=1 SV=1
TMEM109	Transmembrane protein 109 OS=Homo sapiens GN=TMEM109 PE=1 SV=1
NSFL1C	Isoform 2 of NSFL1 cofactor p47 OS=Homo sapiens GN=NSFL1C